



TECHNISCHE  
UNIVERSITÄT  
WIEN  
Vienna University of Technology

## Master's Thesis

# Performance evaluation of DFB gas generation based on a comparison of two research plants with 100 kW and 1 MW

ausgeführt zum Zwecke der Erlangung des akademischen Grades eines Diplom-Ingenieurs  
(Dipl.-Ing oder DI), eingereicht an der TU Wien, Fakultät für Maschinenwesen und  
Betriebswissenschaften, von

**Daniel HOCHSTÖGER**

Mat.Nr.: 11710295

unter der Leitung von

Univ. Prof. Dipl.-Ing. Dr. techn. Hermann Hofbauer

und der Betreuung von

Univ. Lektor Dipl.-Ing. Dr. techn. Matthias Kuba

Institut für Verfahrenstechnik,

Umwelttechnik und Technische Biowissenschaften

E 166

Wien, Jänner 2023



Die approbierte gedruckte Originalversion dieser Diplomarbeit ist an der TU Wien Bibliothek verfügbar  
The approved original version of this thesis is available in print at TU Wien Bibliothek.

---


# Eidesstattliche Erklärung

---

Ich erkläre an Eides statt, dass die vorliegende Arbeit nach den anerkannten Grundsätzen für wissenschaftliche Abhandlungen von mir selbstständig erstellt wurde. Alle verwendeten Hilfsmittel, insbesondere die zugrunde gelegte Literatur, sind in dieser Arbeit genannt und aufgelistet. Die aus den Quellen wörtlich entnommenen Stellen, sind als solche kenntlich gemacht.

Das Thema dieser Arbeit wurde von mir bisher weder im In- noch Ausland einer Beurteilerin/einem Beurteiler zur Begutachtung in irgendeiner Form als Prüfungsarbeit vorgelegt. Diese Arbeit stimmt mit der von den Begutachterinnen/Begutachtern beurteilten Arbeit überein.

Ich nehme zur Kenntnis, dass die vorgelegte Arbeit mit geeigneten und dem derzeitigen Stand der Technik entsprechenden Mitteln (Plagiat-Erkennungssoftware) elektronisch-technisch überprüft wird. Dies stellt einerseits sicher, dass bei der Erstellung der vorgelegten Arbeit die hohen Qualitätsvorgaben im Rahmen der geltenden Regeln zur Sicherung guter wissenschaftlicher Praxis „Code of Conduct“ an der TU Wien eingehalten wurden. Zum anderen werden durch einen Abgleich mit anderen studentischen Abschlussarbeiten Verletzungen meines persönlichen Urheberrechts vermieden.

  
Daniel Hochstöger BSc.

Vienna, January 2023



Die approbierte gedruckte Originalversion dieser Diplomarbeit ist an der TU Wien Bibliothek verfügbar  
The approved original version of this thesis is available in print at TU Wien Bibliothek.

---

# Abstract

---

The fatal consequences of climate change highlight the importance of research into alternative energy sources. Biomass, whether wood or waste materials, can make a significant contribution to independence from fossil fuels. At TU Wien there is a 100kW DFB steam gasification pilot plant which has already been operated numerous times and thus, a comprehensive set of research results are available. Additionally, at the research location of BEST Bioenergy and Sustainable Technologies GmbH at Simmeringer Haide, a 1 MW gasification plant with additional product gas and flue gas cleaning section has been completed on a demonstration scale.

This work deals with the evaluation of the first continuous operation of 1 MW plant with focus on the performance. For the evaluation, the recorded temperature and pressure profile of nearly 6 hours of operation was analyzed. Additionally, performance is determined on the basis of performance indicators and product gas composition. When comparing the results to previously typical results, considerable deviations were found, which are discussed in this master thesis. In addition, further challenges during commissioning, such as undersized screw conveyors and problems with emergency flushing are discussed. In order to be able to quantify future operation modes, reference values are given and performance indicators, which can already be of benefit during operation, are explained. The discrepancies of these data with already existing results are reflected in summary and possible solutions for future research work on the 1MW DFB steam gasifier are elaborated.



Die approbierte gedruckte Originalversion dieser Diplomarbeit ist an der TU Wien Bibliothek verfügbar  
The approved original version of this thesis is available in print at TU Wien Bibliothek.

---

# Kurzfassung

---

Die fatalen Folgen des Klimawandels machen deutlich, wie wichtig die Forschung nach alternativen Energiequellen ist. Biomasse, ob in Form von Holz oder Abfallstoffen, kann dabei maßgebend zur Unabhängigkeit von fossilen Brennstoffen beitragen. Auf der TU Wien befindet sich eine 100kW DFB Dampf Gaserzeugungsanlage, durch welche bereits unzählige Forschungsergebnisse hervorgingen. Am Forschungsstandort der BEST Bioenergy and Sustainable Technologies GmbH auf der Simmeringer Haide wurde darüber hinaus eine 1 MW-Gaserzeugungsanlage mit zusätzlicher Produktgas- und Rauchgasreinigungsstrecke im Demonstrationsmaßstab fertig gestellt.

Diese Arbeit befasst sich mit der Auswertung des ersten Dauerbetriebs dieser 1 MW Anlage mit Fokus auf die Performance. Für die Auswertung wurde der aufgezeichnete Temperatur- und Druckverlauf von knapp 6 Stunden Betriebszeit analysiert. Darüber hinaus wird die Leistung auf der Grundlage von leistungsindikativen Kennzahlen und der Produktgaszusammensetzung bestimmt. Beim Vergleich der Resultate zu bisher typischen Ergebnissen ergaben sich beachtliche Abweichungen, auf welche in dieser Masterarbeit eingegangen wird. Zusätzlich wird auf weitere Herausforderungen während der Inbetriebnahme, wie unterdimensionierte Schneckenförderer und Probleme mit Notspülungen hingewiesen. Um zukünftige Betriebsarten quantifizieren zu können, wird auf Richtwerte eingegangen und leistungsindikative Kennzahlen, welche bereits während des Betriebs von Nutzen sein können, werden erklärt. Die Diskrepanzen dieser Resultate mit bereits bestehenden Ergebnissen werden zusammenfassend reflektiert und Lösungsansätze für zukünftige Forschungsarbeiten am 1MW DFB Gaserzeuger erarbeitet.

---

# Contents

---

<b>Eidesstattliche Erklärung</b>	<b>i</b>
<b>Abstract</b>	<b>iii</b>
<b>Kurzfassung</b>	<b>v</b>
<b>1 Introduction</b>	<b>1</b>
1.1 Dual fluidized bed (DFB) gasification . . . . .	2
1.2 Aim of the work . . . . .	4
<b>2 Materials and Methods</b>	<b>5</b>
2.1 Improvements in recent years . . . . .	5
2.2 Description of the 1MW DFB plant . . . . .	7
2.2.1 Fuel feed to the gasification reactor . . . . .	7
2.2.2 Gasification . . . . .	8
2.2.3 Product gas cooling and cleaning . . . . .	9
2.2.4 Flue gas cooling and cleaning . . . . .	9
2.2.5 Gas utilization . . . . .	9
2.3 Changes in comparison to 8MW DFB gasification plant in Güssing . . . . .	10
2.3.1 Constrictions at the gasification reactor . . . . .	12
2.3.2 Position of fuel feeding . . . . .	12
2.3.3 Utilization of product gas . . . . .	13
2.3.4 Cyclone separators at exhaust- and product gas sections . . . . .	13
2.3.5 Hot gas filter at product gas purification section . . . . .	14
2.3.6 Quench at product gas purification section . . . . .	14



2.3.7	Adjustment of the cross section . . . . .	14
2.3.8	Gravity separator for less abrasion resistant bed material . . . . .	15
2.4	Heating-up process . . . . .	16
2.5	Performance indicating key figures . . . . .	17
2.6	Ash analysis . . . . .	20
2.7	Commissioning difficulties . . . . .	20
2.7.1	Hardened limestone . . . . .	20
2.7.2	Abrasive damage of thermocouple . . . . .	20
2.7.3	Superheater leaking . . . . .	21
2.7.4	Defect cellular wheel . . . . .	21
2.7.5	Undersized screw conveyor motors . . . . .	21
2.7.6	Condensed water in steam supply pipes . . . . .	21
2.7.7	Failure of gas measuring device . . . . .	22
2.7.8	Manual control . . . . .	22
2.7.9	Incorrect calibration data . . . . .	22
2.7.10	Impacts of the difficulties on operation and results . . . . .	23
<b>3</b>	<b>Results</b>	<b>25</b>
3.1	Analysis of high grade wood chips . . . . .	25
3.2	Used bed material . . . . .	27
3.3	Flow diagram and measuring points . . . . .	27
3.4	Duration of commissioning . . . . .	30
3.5	Data from 15.03.2022 . . . . .	32
3.6	Modifications and changes during 11:15 - 17:00 . . . . .	34
3.7	Process flow diagram of reactors . . . . .	34
3.8	IPSEpro Simulation results . . . . .	35
3.9	Product gas composition at different measurement points . . . . .	40
3.10	Ashfraction analysis . . . . .	41
3.10.1	First ash sampling point . . . . .	41
3.10.2	Second ash sampling point . . . . .	42
<b>4</b>	<b>Discussion</b>	<b>45</b>
4.1	Comparison of wood chips and typical wood pellets . . . . .	45

4.2	Analyzing the chosen constant operation point on 15.03.2022 from 11:15 to 17:00	46
4.2.1	Analyzing temperature profile of GR between 11:15 to 17:00 . . . . .	47
4.2.2	Analyzing pressure profile of GR between 11:15 to 17:00 . . . . .	47
4.2.3	Analyzing temperature profile of CR between 11:15 to 17:00 . . . . .	48
4.3	Evaluation of the performance indicating key figures . . . . .	49
4.3.1	Evaluation of water conversion rate . . . . .	49
4.3.2	Evaluation of logarithmic deviation from CO-Shift eq. . . . .	50
4.3.3	Evaluation of product gas yield . . . . .	50
4.3.4	Evaluation of cold gas efficiency . . . . .	51
4.3.5	Evaluation of char combusted in combustion chamber . . . . .	52
4.3.6	Evaluation of air ratio in combustion reactor . . . . .	52
4.3.7	Helpful PIKF for comparison . . . . .	52
4.4	Evaluation of product gas composition . . . . .	54
4.4.1	Evaluation of CO, CO <sub>2</sub> , H <sub>2</sub> and CH <sub>4</sub> contents . . . . .	54
4.4.2	Evaluation of dust, fly char and water content . . . . .	57
4.4.3	Evaluation of NH <sub>3</sub> content . . . . .	57
4.4.4	Evaluation of H <sub>2</sub> S content . . . . .	58
4.5	Further anomalies that occurred during evaluation periode . . . . .	59
4.6	Future DFB gasification in Simmering . . . . .	59
4.6.1	Reliable calibration of the fuel dosing screws . . . . .	60
4.6.2	Indicative values for a promising operation . . . . .	61
4.6.3	Correct part load operation . . . . .	61
<b>5</b>	<b>Conclusion and Outlook</b>	<b>63</b>
<b>6</b>	<b>Notation</b>	<b>65</b>
6.1	Chemical reactions . . . . .	65
6.2	Symbols . . . . .	67
6.3	Abbreviations . . . . .	68
	<b>List of Figures</b>	<b>69</b>
	<b>List of Tables</b>	<b>71</b>
	<b>Bibliography</b>	<b>73</b>

## Chapter 1

---

# Introduction

---

Since global temperatures increase and subsequently climate conditions deteriorate, it is a desire to reduce green house gas emissions. For this reason, in 2015, the Paris-agreement was adopted. A frequently discussed article in the agreement is article 2, sub-point a.:

"Holding the increase in the global average temperature to well below 2 °C above pre-industrial levels and pursuing efforts to limit the temperature increase to 1.5 °C above pre-industrial levels, recognizing that this would significantly reduce the risks and impacts of climate change".[1]

The global average temperature (GAT) is defined as a weighted blend of data sets of surface air temperature and surface sea temperature.[2] Pre-industrial times are commonly used as a reference value in this context and refer to the period between 1880-1920. Figure 1.1 displays the GAT as a function of time (1880-2016). From 1970 the GAT increased continuously and thus peaked in 2016. Fluctuations over the years and the rapid increase in 2016 are primarily influenced by El Niño, a weather anomaly that affects wind and ocean circulation, increasing GAT for some months.[3]

Related to the pre-industrial levels, the GAT increase is 1.26°C at the peak (2016). In contrast to the Kyoto Protocol, the countries that agreed to the Paris agreement set themselves goals every 5 years, which need to be achieved. A specially selected committee for the Paris Agreement will assist the parties in achieving their goals, but there are no penalties for non-achievement.[1]

Decisive sectors in which carbon emissions need to be reduced are for example electricity power, heat production and mobility. To produce the necessary forms of energy sustainably, the countries have to turn away from fossil fuels. Wind, water and solar energy are already used on

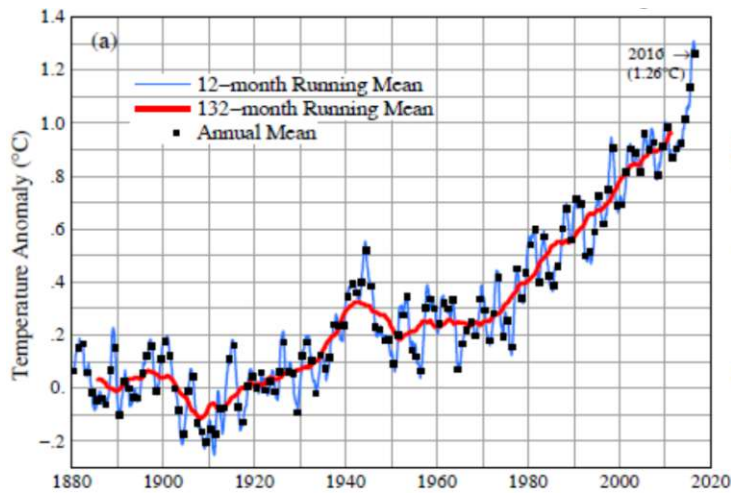


Figure 1.1: Global surface temperatures relative to 1880-1920 based on GISTEMP data, which employs GHCN.v3 for meteorological stations, NOAA ERSST.v4 for sea surface temperature, and Antarctic research station data[4]

an industrial scale. In addition to these sustainable energy sources, biomass has the potential to contribute to independence from fossil fuels. One way to use the energy stored in biomass is the generation of product gas in a dual fluidized bed (DFB). Plants in e.g. Oberwart, Güssing, Senden and Chalmers already tested the functionality of the DFB gasification system multiple times with wood chips as feedstock.[5] Many years of research at 100kW DFB gasification plant at TU Wien brought process advances in design, modes of operation, and materials science. After numerous successful hours of operation on this laboratory plant with different biogenic residues as feedstock, a scale-up to 1MW was undertaken by BEST Bioenergy and Sustainable Technologies GmbH to push the technology one step closer to industrial implementation.

## 1.1 Dual fluidized bed (DFB) gasification

DFB gasification plants consist of a gasification reactor (GR) and combustion reactor (CR). Like shown in Fig. 1.2, the product gas from such gasification primarily consists of hydrogen ( $H_2$ ), carbon monoxide (CO), carbon dioxide ( $CO_2$ ), methane ( $CH_4$ ) and a certain amount of hydrocarbons.[6] Product gas is obtained from the GR by an endothermic conversion of the utilized solid fuel, gasification agent and bed material under thermal influence. A commonly used gasification agent, which was also used in the test series of this master's thesis, is steam. By using steam as gasification agent, nitrogen-free product gas is produced.[7] Further possible gasification agents would be  $CO_2$ [8], air and  $O_2$ . The thermal energy is provided by the

circulating bed material. Commonly used bed materials are silicate sand[9], or the catalytically active bed materials olivine[10] and limestone[7]. By feeding fuel to the gasification reactor, a devolatilization process takes place. Volatile gases and part of the char are entrained by the up-flowing steam and form the basis for the product gas. At the bottom of the GR, bed-material and the rest of the char flows to the CR. In combustion reactor mainly char is used as fuel. Adding combustion air (usually preheated) causes exothermic combustion of the char, releasing heat for bed material heating. Since loop-sealing systems prevent from gas-exchange between the reactors, air can be used for fluidization in the CR without contaminate the GR with nitrogen.[11] Thus, flue gas like nitrogen ( $N_2$ ), carbon dioxide ( $CO_2$ ), water ( $H_2O$ ) and oxygen ( $O_2$ ) are separated from the bed material in the cyclone and loop-sealing system, which is a significant advantage of DFB gasification in comparison to other gasification processes. So, heated bed material is re-entering the GR for heat supply, while flue gas is exhausted.[6] Product gas can be used to produce electricity through a gas engine, provide heat, produce higher-value fuels like synthetic natural gas (SNG) or Fischer Tropsch diesel via synthesis.[12, 13]

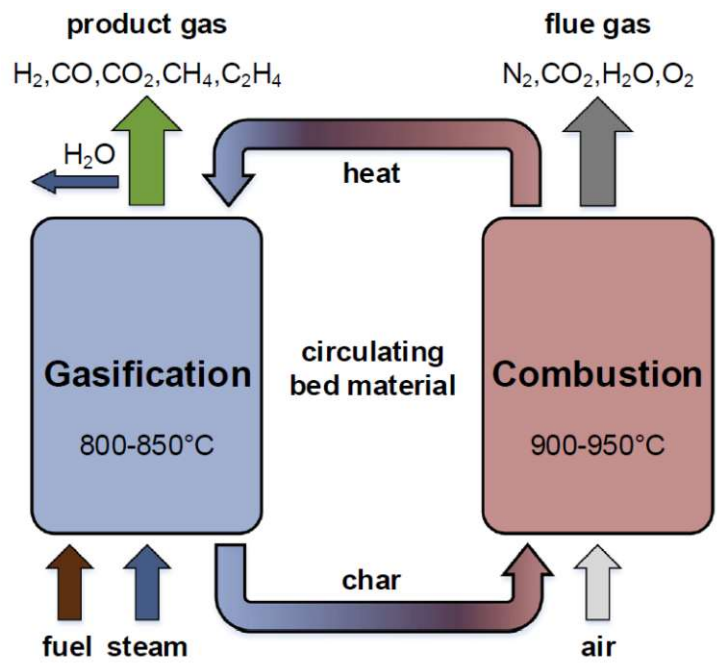


Figure 1.2: Basic principle of the DFB steam gasification process[6]

## 1.2 Aim of the work

With the help of the measurement results obtained in the course of this work, the following questions will be answered:

- How can anomalies that have occurred in terms of temperature, pressure, performance indicating key figures (PIKF) and product gas composition be explained?
- How did the commissioning of the advanced 1 MW dual fluidized bed steam gasification plant compare to design values and the 100 kW plant at TU Wien in terms of PIKF and product gas quality?
- Which values or PIKF will be main indicators for a successful operation in the future?
- How can the new 1MW DFB gasification plant be operated correctly at partial load?

## Chapter 2

---

# Materials and Methods

---

## 2.1 Improvements in recent years

Since about 30 years TU Wien and other universities are researching on DFB gasification.[14] During this period, different optimization measures enhanced this process. Some of these improvements and knowledge are listed in the following points:

- The dependence of some parameters on the bed material particle size was researched by Koppatz et al. in 2012.[15] A summarized overview is given:
  - Fine particle inventory leads to higher turbulence in comparison with coarse particle inventory.
  - In combination with a higher steam-to-fuel ratio, the hydrogen yield is slightly enhanced.
  - Product gas composition is mostly independent from particle size.
  - Tar content in product gas is significantly decreased for fine particle inventory.
- Enhanced DFB gasification reactors are divided into a lower- and upper gasification reactor, as schematically depicted in Figure 2.1. The lower GR is operating as bubbling fluidized bed for devolatilization and gasification of the solid fuel at 750-850°C. In the upper GR higher temperatures occur (900-970°C), which affect reforming and tar cracking processes.[16]

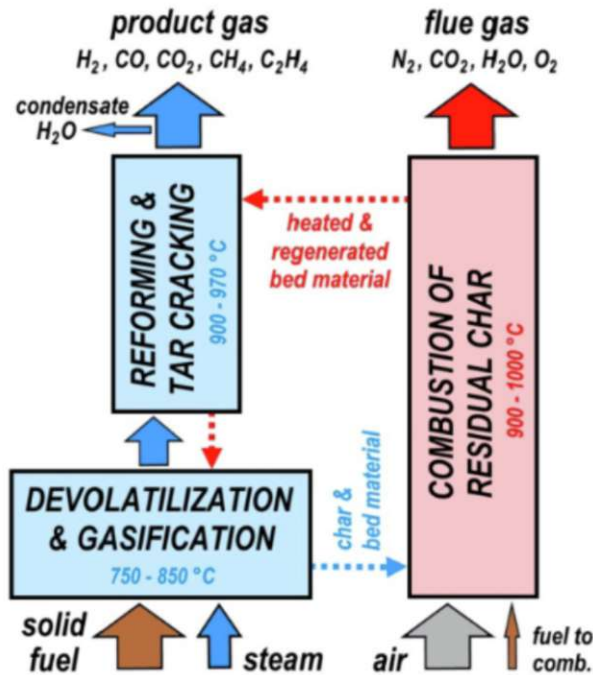


Figure 2.1: Enhanced principle of the DFB steam gasification process[16]

- Catalytic bed materials increase tar cracking and modify product gas composition.[11]
  - Limestone, for example, has an high catalytic effect and provides a hydrogen-rich product gas. Due to the low attrition-resistance of limestone, bed material particles shrink and are more easily entrained with flue gases. This disadvantage can be countered by the use of a gravitation separator instead of a cyclone.[17]
  - Olivine is a commonly used bed material for DFB gasification. Compared to limestone, it has higher attrition-resistance. During the gasification process, olivine generates a calcium-rich inner and outer ash-layer, which has a positive catalytic effect. For example, it enables the reaction with  $\text{CO}_2$ [18] forming  $\text{CaCO}_3$  Kirnbauer2013, and reduces the amount of aromatic tars in the product gas by enhancing the catalytic conversion of aromatic compounds and even preventing their formation.[10]
- Constrictions divided on the height of the upper gasification reactor provide a great impact on the product gas composition and enhance tar cracking. The reason for this is an increased contact between solids and product gas.[16, 19]
- A higher gasification reactor leads to an increased  $\text{H}_2$  content in the product gas. The GR height has a higher impact when non-catalytic bed material is utilized, according to Mauerhofer et al.[16]



## 2.2 Description of the 1MW DFB plant

Based on many years of research at TU Wien, a 1MW DFB gasification plant was designed, constructed and finished at the BEST Bioenergy and Sustainable Technologies site at Simmeringer Haide in January 2022. A direct comparison between the 100kW laboratory DFB gasification plant of TU Wien in terms of space is difficult, because the gasification plant in Simmering is a pre-industrial demonstration plant. Thus, the 1MW DFB gasification plant in Simmering is extended by a laborious gas cleaning system and other plant components. For this, the two gravity separators, which were installed at the laboratory plant at TU Wien for softer bed material, were not installed at the demonstration plant. The reason for this decision is the immense amount of space that a gravity separator on this scale would require. In addition, the gravity separators need a lining. Thereby, the heaviest component would be at the highest point of the plant, which would cause stability problems. For utilization of the product gas in a gas engine or boiler, the realized cleaning components would be sufficient. Nevertheless, further cleaning components would be necessary in Simmering to use the product gas as a synthesis gas. In following, the process of gas production and the plant components are described. Figure 2.3 is intended to provide a basis of understanding and assigns the components by concrete designation.

### 2.2.1 Fuel feed to the gasification reactor

The biomass is delivered in dry form in two walking floor containers (90-B01, 90-B02) to the dual fluidized bed (DFB) gasification plant. One of the two containers is supplying the feedstock for the gasification process, while the other one can be filled. Via a conveyor belt (92-H01) the feedstock is brought to the reverse system (93-H01), which is used to fill up the two bunkers (94-B01, 94-B02). The fuel in the two bunkers enters the feeding screw (95-H01) via the corresponding dosing screw (94-H01, 94-H02), where the fuels can be blended if desired. To prevent backflow, the fuel is pushed by the feeding screw into the double rotary feeder (96-X01) before entering the gasification reactor (60-R01). In addition, due to the on-bed feeding system, the feedstock is not in direct contact with the hot atmosphere of the gasification reactor. Thereby, different waste fractions with lower melting points can be utilized.[6]

## 2.2.2 Gasification

In addition to fuel, bed material from the upper gasification reactor (upper GR, 60-R02)[16], separated bed material from the radiation cooler (70-K01, 70-K02) and steam is entering the reducing atmosphere of the lower gasification reactor (lower GR, 60-R01). There, devolatilization and gasification reactions occur. The lower gasification reactor is operating as a bubbling fluidized bed and has a rectangular cross section, which enlarges towards the top. The gas mixture flows from the lower to the upper GR, where it further reacts with incoming steam due to heat supply through the bed material. A siphon is used to transport bed material from the combustion reactor to the upper GR, without transferring air or flue gas.[20] The upper GR is operating in counter current flow. Thus, hot bed material coming from the cyclone is flowing downwards, while product gas and tars are streaming upwards. Over the height, the upper GR has five constrictions, that create locally smaller diameters and ensure a higher turbulence, resulting in an enhanced contact between gas and solid particles. As a result, more tars are getting reformed and catalytically activated bed material promotes reforming reactions. Due to the absence of air, a nitrogen free product gas is generated. The product gas streams with a part of the fine bed material and tars on to the radiation cooler (70-K01, 70-K02).

Cooled bed material and part of the char (unconverted fuel), leave the lower gasification reactor (60-R01) via a chute and enter the oxidizing atmosphere of the combustion reactor (61-R01), where the char is burned and the cooled bed material reheated. Because of the constant attrition of bed material in the fluid bed components, the bed material is getting smaller. As a result, it is more likely that bed material is entrained by the product gas and the flue gas. Unused bed material can be fed to the combustion reactor via flow bin (61-B01, 61-B02). Instead of bed material, the flow bin can be filled with pellets for additional heating during heating up process. Combustion air is added on the bottom of the combustion reactor. Distributed over the height of the combustion reactor, heated air is added on two further locations for an enhanced burning reaction. Furthermore, fly char from the cyclone (71-C01) and the hot gas filter (72-F01) of the product gas cleaning line is added. For additional heat supply during gasification process, heating oil, emulsion from the biodiesel-phase separator and air can be fed to the combustion reactor via the heating oil lance. To economize heating oil, product gas is recycled in the combustion reactor.

### 2.2.3 Product gas cooling and cleaning

The radiation cooler (70-K01, 70-K02) consists of two pipes, which are cooled from the outside with water. For temperature controlling, the cooling water level of the second pipe can be adjusted. On the lowest point of the radiation cooler, entrained fuel and bed material can be separated and fed back to the lower gasification reactor (60-R01) via two screw conveyors (70-H01, 70-H02). After the radiation cooler, particles are separated in the cyclone (71-C01) and the hot gas filter (72-F01). High filtration temperatures prevent the tars from clogging the filter. Afterwards, the gas is cooled and cleaned from the tars in the first scrubber by water (74-K01) and in the second scrubber by biodiesel (RME-rapeseed oil methyl ester, 75-K01). A phase separator (75-B01) separates RME from water. The so obtained RME circulates between RME-scrubber and phase separator. After several utilization periods, tar-enriched RME-emulsion is replaced. Blended with fuel oil, tar-enriched RME-emulsion gets burned in the combustion reactor for efficiency increase.

### 2.2.4 Flue gas cooling and cleaning

Heated bed material and flue gas from the combustion reactor (61-R01) get separated in a cyclone (63-C01). Flue gas is getting cooled in an adjustable radiation cooler (80-K01, 80-K02) to about 500°C and cleaned from ash in another cyclone (81-C01). The remaining heat is used in a heat exchanger (82-W01) to heat air for the combustion reactor. A redundancy cooler (83-W01) ensures, that the temperature of the flue gas is lower than 180°C, to protect the fabric filter (84-F01). Flue gas is fed to the afterburner (110-B01) for complete oxidation. Subsequently, flue gas from afterburner is used for heating up water from the steam drum in a boiler (110-B02). Fly ash from radiation cooler, cyclone and fabric filter get collected in the flow bin (84-Z02).

### 2.2.5 Gas utilization

From the biodiesel scrubber (75-K01) cleaned product gas streams on to the post-combustion chamber (110-B01) or further gas cleaning units to obtain gas, that is clean enough for synthesis. Exhaust gases from the afterburner chamber are used for steam generation in the boiler (110-B02), which forms a steam-circuit with the steam drum (100-B01). After cooling down, exhaust gas is directed to Wien Energie GmbH, or, in case of emergency, blown out via a blow-out pipe on the roof (110-X01). After the biodiesel scrubber, the online measuring device is attached to

the product gas blower. The offline measuring points can be seen in Figure 3.1.

Figure 2.2 shows the 1 MW DFB steam gasification plant in Simmering at start of operation.



Figure 2.2: 1 MW DFB steam gasification plant in Simmering with project name Waste2Value by BEST-research[21]

## 2.3 Changes in comparison to 8MW DFB gasification plant in Güssing

The DFB gasification demonstration plant in Güssing started its continuous operation in 2002 for about 15 years. In some aspects, the DFB plant in Güssing was the predecessor to Simmering. Since 2002, improvements, like exemplarily given in chapter 2.1, were researched on DFB laboratory gasification plants. The 1MW gasification plant in Simmering is testing these improvements at demonstration scale. While 8MW DFB plant in Güssing only used wood chips as fuel, enhanced 1MW DFB plant at Simmeringer Haide will also gasify residual materials and waste for research purpose.[22]



### 2.3.1 Constrictions at the gasification reactor

Furthermore, last decade brought an interest in cascade use. This means, lower quality fuels like residual waste, sewage sludge and bark should be gasified. Thereby, procurement costs will be reduced. To obtain a sufficient conversion of such fuels, the residence time in the gasification reactor at Simmering is increased with constrictions. These constrictions lead, due to increased turbulence of fuel, bed material and steam, to a longer residence time of the fuel in the reactor and thus to a more complete conversion. In this way, more tars are converted and efficiency is enhanced. Fewer tars in the product gas subsequently result in a relief of the product gas purification section.[16, 19]

### 2.3.2 Position of fuel feeding

Another difference is the fuel feeding. In general, the position of fuel feeding has an influence on product gas composition. In the following, some findings on this topic, which were researched and discussed in more detail by S. Kern et al in 2013, are given.[23] In-bed feeding results in higher H<sub>2</sub> content and less tars. On-bed feeding leads, as shown in Fig. 2.4, to a higher content of CO. Since carbon conversion is enhanced with on-bed feeding, a higher amount of product gas with a higher heating value is produced. The amounts of product gas are compared in Fig. 2.5. For synthesis reactions mostly H<sub>2</sub>:CO ratio >2 and low amounts of tars are necessary. Thus, for generation of product gas, as in Simmering, in-bed feeding is preferred. For CHP processes, as in Güssing, higher heating values are desired, which are reached with on-bed feeding.[23]

Güssing supplied the fuel with an in-bed feeding system, which was installed for a fast direct contact between bed material and fuel. This configuration resulted in a permanent pressure on the screw by the bed material. In addition, pyrolysis of fuel already took place before the screw outlet. Condensation of the released gases on the outer wall of the screw resulted in clogging. In Simmering, an on-bed feeding system is used. So the filled feeding screw is not heated by the hot atmosphere of the gasification reactor. To accomplish on-bed feeding, fuel is fed on the edge of the lower gasification reactor.[22]

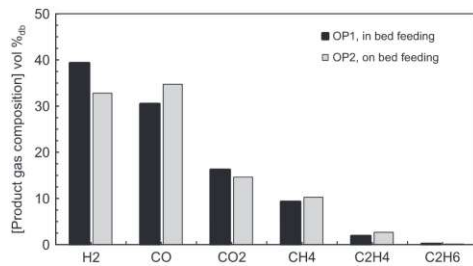


Figure 2.4: Measured permanent gas composition of the product gas[23]

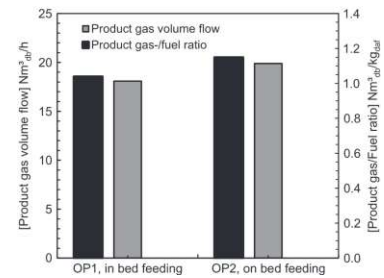


Figure 2.5: Total and specific gas production[23]

### 2.3.3 Utilization of product gas

The gasification plant in Güssing was designed as CHP (Combined Heat and Power) plant. To use the obtained product gas in a gas engine and further a heat exchanger, product gas requirements are moderate. Thus, the product gas section in Güssing consists of a heat exchanger to cool the product gas, a bag filter to separate particles, and a biodiesel (RME-rapeseed oil methyl ester) scrubber to separate tars. In Simmering, product gas flows through a more elaborate purification process. The intention is to produce synthesis-capable gas that can, after several more steps of cleaning, be utilized in the laboratory at the location. To achieve this, the generated product gas first flows, as described in more detail in chapter 2.2, through an adjustable radiation cooler. Afterwards, it is cleaned from particles in a cyclone and ceramic candle filter before being freed from tars in the quench and RME scrubber. It is necessary to separate tars and sulphur compounds to prevent clogging and deactivation of the catalyst.[22]

### 2.3.4 Cyclone separators at exhaust- and product gas sections

In order to relieve hot gas filter in product gas section and heat exchanger and fabric filter in exhaust gas section, cyclone separators are installed in Simmering before the respective apparatuses. This cyclone separates coarse material at a size  $>0.1\text{mm}$ . Thus, less Pulse-Jets are necessary. In this way, operating time of filter candles and tubes are increased and thus, maintenance costs are reduced.[22]

### **2.3.5 Hot gas filter at product gas purification section**

In Güssing, the product gas is cooled down to be subsequently cleaned in a fabric filter. This fabric filter is pre coated with limestone, so the condensed tars do not clog the filter. At DFB gasification plant in Simmering, a hot gas filter is installed in product gas section. Thus, the tars mainly will not condense and remain in product gas, preventing the hot gas filter from clogging.[22]

### **2.3.6 Quench at product gas purification section**

To remove tars from product gas, RME (rapeseed oil methyl ester) scrubber was utilized in Güssing. Simmering is utilizing quencher and RME scrubber. As RME has a flash point of 91-135°C, it is necessary to cool down the product gas first.[24] So, the still hot product gas in Simmering is cooled by a quench, whereby tars condense. The main component of tar-purification section in Simmering is a scrubber operating with RME. These separated tars, in the form of an emulsion, are recycled back to the combustion reactor and thus increase efficiency.

### **2.3.7 Adjustment of the cross section**

Additionally, an enhanced cross section of the gasification reactor is installed in Simmering. Due to the volatile gases emitted by the fuel, the cross-section of the lower gasification reactor tapers conically in the middle segment. While the gasification reactor in Güssing has an asymmetric conical cross section, the gasification reactor in Simmering is symmetric conical. This is illustrated schematically in Figure 2.3 at the lower gasification reactor (60-R01). As a result, enhanced fluidization and subsequently a more complete gasification reaction of the biomass particles is reached.[25]

Table 2.1 presents an overview of the points mentioned in this chapter. In summary, there are seven main differences between Simmering and Güssing. These differences are intended to make the process more efficient. Some of these improvements were tested in previous experiments at the 100kW laboratory plant of TU Wien.



### 2.3.8 Gravity separator for less abrasion resistant bed material

Another discussed enhancement option were the gravity separators, which were tested at 100kW DFB gasification plant at TU Wien. These separators were installed after the combustion and the gasification reactor. The reason for this enhancement was the use of catalytic more effective bed material like limestone, which is not enough resistant against attrition in cyclone. To use this separation method in upscaling, the gravity separator vessels would have been too big and additionally at the highest point of the gasification plant.[7, 26]

Nevertheless, in Simmering, coarse particles sink to the bottom in the first reversal of the product gas radiation cooler due to gravity and are returned to the gasification reactor by two feeding screws.

	Güssing	TU Wien	Simmering
Constrictions in GR	-	•	•
On - bed feeding	-	•	•
Utilization as synthesis gas	-	-	•
Cyclone separator at exhaust- and product gas section	-	n.p.	•
Hot gas filter at product gas section	-	n.p.	•
Quench at product gas section	-	n.p.	•
Symmetric conical GR	-	•	•
Gravity separator for less abrasion resistant bed material	-	•	-

- ... installed
- ... not installed
- n.p. ... no purification section

Table 2.1: Comparison of the DFB gasification plant design of different locations

## 2.4 Heating-up process

Heating up the gasification plant for the first time requires a precisely regulated heating curve, like shown in Figure 2.6. This heating scheme is prescribed by the Vienna based company Rath AG, which supplies refractory products, systems and services. Before the start of heating, the plant should air-dry for 24 hours. If the first heating-up process is interrupted for operational reasons and there is a significant drop in the oven temperature, the heating process can be continued at the actual oven temperature. The reason for this procedure are the water deposits in the refractory lining, which need to be drained slowly to avoid cracks. Refractory lining should generally be protected against direct water ingress.

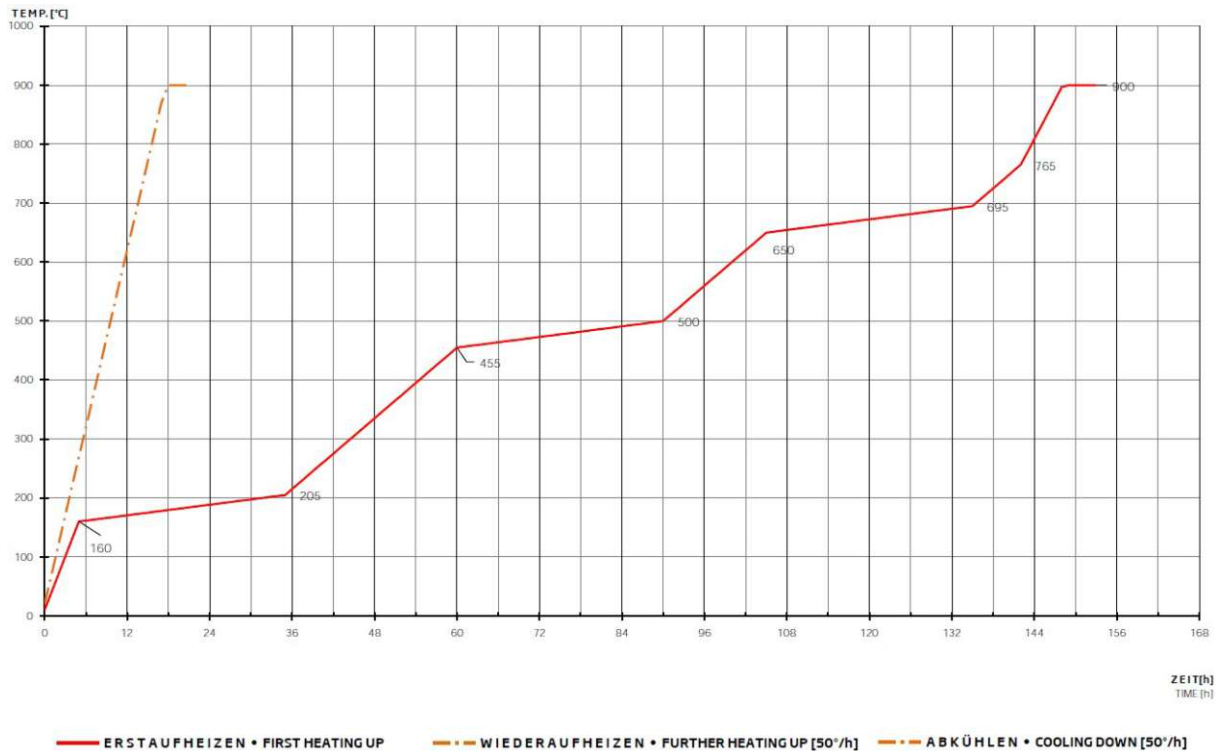


Figure 2.6: Heating-up scheme

The first-heating-up line is divided into steep and flat sections. Table 2.2 illustrates the given scheme in numbers. The total time required for first heating-up process is 149h without maintenance. Operational reasons (e.g. fallen electric fuse, blockage of cellular wheel, fluidized bed failure etc.) resulted in a total heating time of about 3.5 weeks to reach the operating temperature of 900°C. After this time, on 09.02.2022, the DFB gasification plant in Simmering started operation.

	Time [h]	Temperature [°C]	Heating rate [K/h]
1	0	10	-
2	0-5	160	30
3	5-35	205	1.5
4	35-60	455	10
5	60-90	500	1.5
6	90-105	650	10
7	105-135	695	1.5
8	135-142	765	10
9	142-148	897	22
10	148-149	900	3

Table 2.2: Heating-up rate

In general, the heating process was based on the hottest temperature in the DFB circuit. A close attention was focused on temperature sensor 61TICZA-030, which is installed between secondary- and tertiary air supply. Up to 400°C was heated electrical. Subsequently, wood pellets were used for heating up to around 750°C. Then, fuel oil heated the plant to operating temperature.

A premature use of fuel oil is not possible, because there is no ignition source at the fuel oil lance. An ignition source would need to be monitored, which is not possible in a fluidized bed due to abrasion. As assumed, auto ignition temperature of fuel oil depends on temperature and pressure and can therefore vary significantly in the fluidized bed reactor. To avoid agglomeration of fluid fuel oil in the CR or, even worse, in gaps of the lining, fuel oil is only used from a reactor temperature of 750°C upwards. At this temperature and above, it can be assured that the fuel oil will ignite when entering the reactor atmosphere.

## 2.5 Performance indicating key figures

At present, the system does not provide a simultaneous evaluation of the data. Thus, raw data of the operation is recorded and subsequently analyzed in IPSEpro. Raw data include temperature and pressure measurements of the installed sensors. In addition, flow measurements and recorded setting values provide information on material input and output from the individual subsystems e.g. steam, air and fuel input. An online measuring device provides information on the hydrogen, carbon monoxide, carbon dioxide and methane content in the product gas. Another online measuring device provides information on the exhaust gas composition after the exhaust gas

purification section. IPSEpro uses the data in a process simulation model to calculate mass and energy balances for the entire system in order to subsequently generate unknown values.

The following performance indicating key figures were calculated by applying the process simulation program IPSEpro. These parameters are used for comparison of DFB gasification plants with different sizes or different operation conditions and are mostly unitless.[6]

Eq. 2.1 calculates the steam to fuel ratio  $\Phi_{SF}$ . The total steam supplied is the sum of steam from fluidization and water, which enters the GR with the fuel. The inserted mass flow rate of fuel is taken dry and ashfree.

$$\Phi_{SF} = \frac{\dot{m}_{steam,GR} + \dot{m}_{H_2O,GR,fuel}}{\dot{m}_{GR,fuel,daf}} \quad (2.1)$$

With Eq. 2.2 steam to carbon ratio  $\Phi_{SC}$  is calculated. This unitless figure is useful for comparing test runs with different fuels.

$$\Phi_{SC} = \frac{\dot{m}_{steam,GR} + \dot{m}_{H_2O,GR,fuel}}{\dot{m}_{C,GR,fuel}} \quad (2.2)$$

The ratio between the volume flow of dry product gas to dry and ashfree introduced fuel is named product gas yield and is given in Eq. 2.3.

$$PGY = \frac{\dot{V}_{PG}}{\dot{m}_{GR,fuel,daf}} \quad (2.3)$$

With Eq. 2.4 absolute steam-related water conversion  $X_{H_2O,abs}$  is given. The equation relates the consumed water to the water, that is introduced into the process.

$$X_{H_2O,abs} = \frac{\dot{m}_{steam,GR} + \dot{m}_{H_2O,GR,fuel} - \dot{m}_{H_2O,PG}}{\dot{m}_{steam,GR} + \dot{m}_{H_2O,GR,fuel}} \quad (2.4)$$

Another indicator for water consumption for gasification and steam reforming reactions is the relative water conversion, which can be calculated with Eq. 2.5.

$$X_{H_2O,rel} = \frac{\dot{m}_{steam,GR} + \dot{m}_{H_2O,GR,fuel} - \dot{m}_{H_2O,PG}}{(1 - v_{H_2O} - v_{ash})\dot{m}_{fuel}} \quad (2.5)$$

In general, a high hydrogen content is desirable. To achieve this, the water gas shift reaction (Eq. 6.5) is a decisive reaction in the gasification process. The model parameter  $p\delta_{eq,CO-shift}(p_i, T)$  is a measure of how close to equilibrium the reaction is. This parameter is defined as logarithm of the ratio of the actual partial pressure product to the equilibrium constant and is given with equation 2.6. The equilibrium constant  $K_{p,CO-shift}(T)$  can be determined with a thermochemical simulation software e.g. HSC chemistry.[23]

If the parameter is  $<0$ , the molecules of the reactant side are mainly present. If it is  $>0$ , the products of the reaction are more present.  $p\delta_{eq,CO-shift} = 0$  thus represents the equilibrium.[23]

$$p\delta_{eq,CO-shift}(p_i, T) = \log_{10} \left[ \frac{\prod_i p_i^{v_i}}{K_{p,CO-shift}(T)} \right] \quad (2.6)$$

The cold gas efficiency  $\eta_{CG}$  sets the chemical energy of the product gas and the chemical energy in the fuel in ratio and is given in Eq. 2.7.

$$\eta_{CG} = \frac{\dot{V}_{PG} * LHV_{PG}}{\dot{m}_{GR,fuel} * LHV_{GR,fuel}} * 100 \quad (2.7)$$

The overall cold gas efficiency, which formula is given with Eq. 2.8, additionally considers the fuel which is fed to the CR and heat losses.

$$\eta_{CG,o} = \frac{\dot{V}_{PG} * LHV_{PG}}{\dot{m}_{GR,fuel} * LHV_{GR,fuel} + \dot{m}_{CR,fuel} * LHV_{CR,fuel} - \dot{Q}_{loss}} * 100 \quad (2.8)$$

## 2.6 Ash analysis

Ash analysis and product gas composition, combined with fuel analysis and plant parameters, provides the basic components for understanding the reactions that take place during a process. Ash composition can have a huge impact on process operation. High amounts of potassium and silicon lead to a decrease of ash softening temperature and as a consequence to plugged apparatuses and pipes. Adding limestone or kaolin can counteract this effect.[27]

In addition to ash composition, particle size and extraction point is decisive. This makes it possible to determine which ash fraction is separated at which apparatuses of the purification section. In general, it is advantageous to have as many ash sampling points as possible in order to be able to follow the process properly.

The amount of ash determines the technical requirements necessary to comply with legal emission regulations and to keep environmental pollution low. As the ash content increases, so does the effort required for maintenance work due to the necessary dust removal and disposal or recycling of the ash.

## 2.7 Commissioning difficulties

Before and during the commissioning campaign, several difficulties occurred that affected test execution and measurement results. In the following, some of these occurred difficulties are mentioned.

### 2.7.1 Hardened limestone

During the gasification operation, there was a malfunction of the plant, which caused the exhaust gas to be released to the environment via roof instead of being directed to the rotary kiln. In this case, automatic flushing is activated. The exhaust line was constantly filled and water entered the exhaust gas cleaning sections. As a result, limestone got in contact with water and hardened.

### 2.7.2 Abrasive damage of thermocouple

High fluidization velocities led to abrasive damage of thermocouple through bed material. Especially at top of the combustion reactor high fluidization velocities prevailed. The higher the thermocouple is placed in combustion reactor, more abrasive damage occurred. Therefore, the

top three thermocouples of combustion reactor (61-TISA-050, 61-TICSA-040, 61-TICZA-030) had to be replaced after commissioning. The excentric installation of the thermocouples results in less abrasive impact at the expense of measurement accuracy.

### **2.7.3 Superheater leaking**

Before commissioning, the plant was checked for leaks with air. Only during operation with steam, small leaks were noticed on the superheaters. These leaks were insignificantly low compared to the amount of steam used.

### **2.7.4 Defect cellular wheel**

Due to a defect cellular wheel, the commissioning start was delayed. This cellular wheel was located at the bottom of the cyclone in exhaust gas section. The cellular wheel was still functional before the start of heating. Therefore, it can be assumed that this problem occurred due to thermal expansion. The cell wheel at the bottom of the radiation cooler in the exhaust gas section did not cause any problems at even higher temperatures, which indicates that tolerance inaccuracies exist.

### **2.7.5 Undersized screw conveyor motors**

After commissioning, an attempt was made to remove a part of the bed material for analysis via the outlet screw. Though, the motor of the cooling screw 61-H04 was undersized with 0,37kW. The bed material leaving the bottom of the combustion reactor and enters the cooling screw through a fall pipe, created a blockage in the conveyor. New design considerations resulted in a motor power of about 5kW including safety supplement. After first test runs, also the dosing screw conveyor motors were undersized. These were also replaced before commissioning.

### **2.7.6 Condensed water in steam supply pipes**

Heating oil, fully demineralized water, process water, nitrogen and steam are supplied by Wien Energie GmbH. Cold temperatures in February 2022 led to water condensation in steam supply pipes. This problem occurred only initially, indicating that the pipes had to be warmed up.

### 2.7.7 Failure of gas measuring device

After product gas cleaning section, a small amount of the product gas is diverted and directed to the online gas measuring device. Still remaining tars and dust particles in product gas cause a failure of the gas measuring device. To avoid this failure, fabric filters separate remaining contaminants. These filters need to be replaced after a certain time.

### 2.7.8 Manual control

During commissioning there were no controls and automations available. Control-intensive plant components like product gas blower, product gas recirculation blower or afterburner chamber blower required constant attention. Meanwhile these plant components are pressure-regulated each to a certain pressure measuring point. Furthermore, more frequent inspections were required as no paddle sensors were installed yet in transfer stations (91-H01, 91-H02).

### 2.7.9 Incorrect calibration data

Fuel calibration provided incorrect data. In preparation for commissioning, the two feed bunkers (94-B01, 94-B02) were filled with high-quality wood chips. In order to obtain the fuel mass flow and thus the power supplied to the gasification reactor, the two 50Hz dosing screws of each feed bunker were operated alternately and together at different frequencies and the mass conveyed was recorded in the respective time. The rest of the conveyor line, in this case the feeding screw (95-H01), was run at maximum speed to avoid fuel accumulation. The intention of the calibration is to obtain the fuel mass flow and thus the power fed into the gasification reactor. For this purpose, the calibration opening of the feeding screw (95-H01) on the 2nd floor, which is located after the feed bunkers, was opened. In order to transport the output from the calibration opening into the 60 liter barrel located on the 1st floor in a controlled manner, a big bag was attached to the calibration opening. The measuring time depended on the filling level of the barrel, as it still had to be carried. This occurred to a short measuring time of one to four minutes and further in inaccurate results. Furthermore, a run-in time of 2 minutes would have been necessary to obtain a constant fuel mass flow rate. These reasons led to an incorrect calibration curve, which is shown in Figure 2.7. This Figure shows the actual power supplied (red) and the intended power supplied (blue) in relation to the motor frequency. At 50Hz a motor power of 100% is reached.



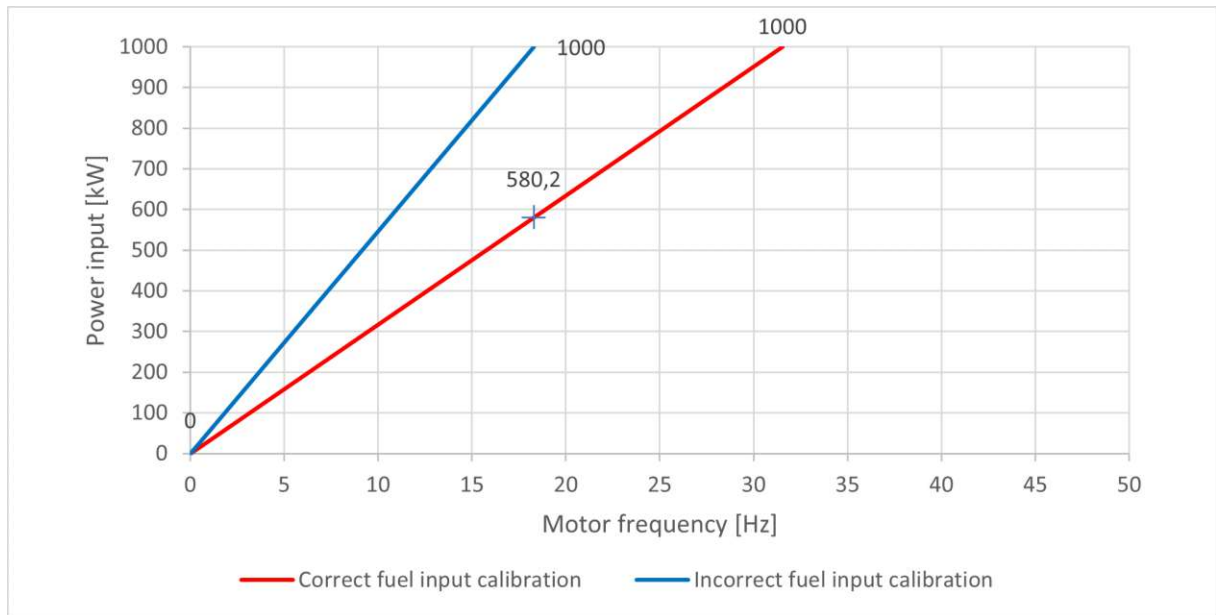


Figure 2.7: Correct and incorrect fuel input comparison with respect to motor frequency

### 2.7.10 Impacts of the difficulties on operation and results

Difficulties such as hardened limestone, abrasive damage to the thermocouples, and superheater leakings did not cause problems that would lead to immediate shutdown of the plant during commissioning, but needed to be fixed afterwards during cleaning and maintenance. Most of the above mentioned difficulties, as defect cellular wheel, undersized screw conveyor motor, condensed water in steam supply pipes, or manual control complicated or delayed operations. The only difficulty with consequences on the whole commissioning and its measuring results was the incorrect calibration data. This led to a permanent partial load operation of the plant and, furthermore e.g., to a high steam to fuel ratio and high heating oil input.



Die approbierte gedruckte Originalversion dieser Diplomarbeit ist an der TU Wien Bibliothek verfügbar  
The approved original version of this thesis is available in print at TU Wien Bibliothek.

## Chapter 3

---

# Results

---

As described in section 2.7, the dual fluidized bed steam gasification plant in Simmering was operated at partial load during commissioning due to calibration failure. For comparison, partial load operations of other DFB steam gasification plants are used at some points of this work. Full- and part load operation at 100kW plant of TU Wien were analyzed by M. Kolbitsch in 2016.[28] Another part load operation of DFB steam gasification took place in Oberwart, Burgenland, at the 8.5MW CHP plant. During a 2250-h long term test run in 2015, where product gas from DFB steam gasification plant is used to operate a water gas shift pilot plant, one of the two gas engines fails for 300 hours, resulting in partial load operation.[29] To generate a discussion base, some characteristics, operating parameters and knowledge of these two operation modes are mentioned in this chapter.

### 3.1 Analysis of high grade wood chips

For the first test series, high grade wood chips were used as fuel. Wood has, with 82%, on average a high amount of volatile components. Ash content of wood is low (<1%). The average composition of coarse wood ash is about 42% CaO, 6% K<sub>2</sub>O, 6% MgO, 3% P<sub>2</sub>O<sub>5</sub> and 1% Na<sub>2</sub>O and small amounts of iron and manganese. In addition, contaminants like quartz sand, soil and stones can be included.[30, 31]

Table 3.1 compares the elemental analysis data of feedstock used at commissioning with typical wood pellets, which M. Kolbitsch used at the 100kW plant for the fuel variation tests.[32] During 2250-h test in Oberwart, several types of wood chips with e.g. different water content were used. Therefore, no specific fuel data is available and commissioning-like analysis data is assumed in the following.[29]

### Fuel analysis

		Commissioning used wood chips	Typical wood pellets
Water content	wt.-%	14.25	7.2
Ash content	wt.-% <sub>db</sub>	0.89	0.2
Carbon content	wt.-% <sub>db</sub>	49.36	50.7
Hydrogen content	wt.-% <sub>db</sub>	5.84	5.9
Nitrogen content	wt.-% <sub>db</sub>	0.14	0.21
Sulfur content	wt.-% <sub>db</sub>	<0.02	0.005
Chlorine content	wt.-% <sub>db</sub>	<0.01	0.005
Content of volatile components	wt.-% <sub>db</sub>	83.86	85.4
Upper heating value H <sub>o</sub>	kJ/kg <sub>db</sub>	19678	-
Lower heating value H <sub>u</sub>	kJ/kg <sub>db</sub>	18395	18940

Table 3.1: Elemental analysis of A. commissioning used high grade wood chips and B. typical wood pellets[33, 32]

Table 3.2 and 3.3 compares elementary compositions and melting characteristics of the ash of commissioning used wood chips with typical wood pellets. In the elementary analysis of the wood pellets, the oxides not mentioned were summarized. These oxides result in a sum of 9.8 wt.-%<sub>db</sub>.

### X-ray fluorescence analysis of the ash

Commissioning used wood chips				Typical wood pellets	
Oxide	wt.-%	Oxide	wt.-%	Oxide	wt.-%
MoO <sub>3</sub>	n.d.	Cr <sub>2</sub> O <sub>3</sub>	n.d.		
Nb <sub>2</sub> O <sub>5</sub>	n.d.	V <sub>2</sub> O <sub>5</sub>	n.d.		
ZrO <sub>2</sub>	n.d.	TiO <sub>2</sub>	n.d.		
SrO	0.2	CaO	46.1	CaO	55.2
PbO	n.d.	K <sub>2</sub> O	28.3	K <sub>2</sub> O	13.4
As <sub>2</sub> O <sub>3</sub>	n.d.	MgO	11.6	MgO	8.3
ZnO	0.1	SO <sub>3</sub>	4.2		
CuO	0.1	P <sub>2</sub> O <sub>5</sub>	4.9	P <sub>2</sub> O <sub>5</sub>	3.1
NiO	n.d.	SiO <sub>2</sub>	3.0	SiO <sub>2</sub>	6.6
Co <sub>3</sub> O <sub>4</sub>	n.d.	Al <sub>2</sub> O <sub>3</sub>	0.3	Al <sub>2</sub> O <sub>3</sub>	1.6
ClO <sub>2</sub>	0.1	Fe <sub>2</sub> O <sub>3</sub>	0.2	Fe <sub>2</sub> O <sub>3</sub>	0.9
MnO	0.2	Na <sub>2</sub> O	0.7	Na <sub>2</sub> O	1.1

n.d. ... not detected

Table 3.2: RFA from A. high grade wood chips used at commissioning and B. typical wood pellets[33, 32]

<b>Ash melting characteristics</b>			
		Commissioning used wood chips	Typical wood pellets
Softening temperature	°C	>1500	1265
Hemisphere temperature	°C	>1500	1273
Flow temperature	°C	>1500	1290

Table 3.3: Analysis of ash melting characteristic of high grade wood chips made by fuel laboratory of TU Wien, released on 01.02.2022 and typical wood pellets analyzed by J.I. Arranz in 2015, COM2[33, 34]

Looking at the three Tables 3.1, 3.2 and 3.3 compared above, common contents are remarkable. The carbon content, which is a determining characteristic for the calorific value, is almost the same. The water content is higher in the wood chips used for commissioning. Potassium oxide in the commissioning wood chips was 28.3%, more than twice as high as in typical wood pellets. In turn, with 3% silicon oxide of typical wood pellets is only half the content in commissioning used wood chips. Ash melting characteristics as softening and flow temperature were higher in the case of commissioning wood chips. Since these values are average compositions of wood chips and wood pellets, they can also be used for comparisons of some other publications.

## 3.2 Used bed material

During commissioning, a 80/20 mixture of olivine and limestone was used as bed material. At the operating point, 1500 kg of bed material, including 1200 kg of olivine and 300 kg of limestone, were filled in the gasification plant at Simmeringer Haide. For IPSEpro analysis, no additional bed material was fed to the system during operation. Table 3.4 below lists typical parameters of the used bed material. Additionally, a sample illustrates both materials, olivine and limestone, beside the Table.

## 3.3 Flow diagram and measuring points

The process flow diagram of the 1MW advanced DFB demonstration plant at Figure 3.1, which is taken over from simulation report of TU Wien, provides a good overview of the two reactors and the gas cleaning sections. The design was already described at section 2.2. This process flow diagram is divided into three parts. The first part schematically depicts the gasification process with its main inputs for gasification operation as biomass, steam, combustion air and recycled

Olivine



Limestone



### Olivine

Parameter	Unit	Value
SiO <sub>2</sub>	[wt.-%]	39-42
Fe <sub>2</sub> O <sub>3</sub>	[wt.-%]	8-10,5
MgO	[wt.-%]	48-50
Hardness	Mohs	6-7
Sauter mean diameter	µm	250
Particle density	kg/m <sup>3</sup>	2900

### Limestone

Parameter	Unit	Value
CaCO <sub>3</sub>	[wt.-%]	95-97
MgCO <sub>3</sub>	[wt.-%]	1,5-4
SiO <sub>2</sub>	[wt.-%]	0,4-0,6
Hardness	Mohs	3
Sauter mean diameter	µm	480
Particle density	kg/m <sup>3</sup>	2650, *1500

\* ... Particle density after full calcination

Table 3.4: Average compositions of olivine and limestone with exemplary illustration aside [18, 33]

fuel from downstream plant components as fly char, RME-emulsion and product gas. Second part shows the gas cooling and cleaning sections of gasification and combustion chain. In and outputs are labeled as well. Third part is captioned as product gas recycling and burning and focuses on the post combustion chamber of the product gas. In addition, the measuring points are marked pink and named in the process flow diagram, which will be used in further sections.

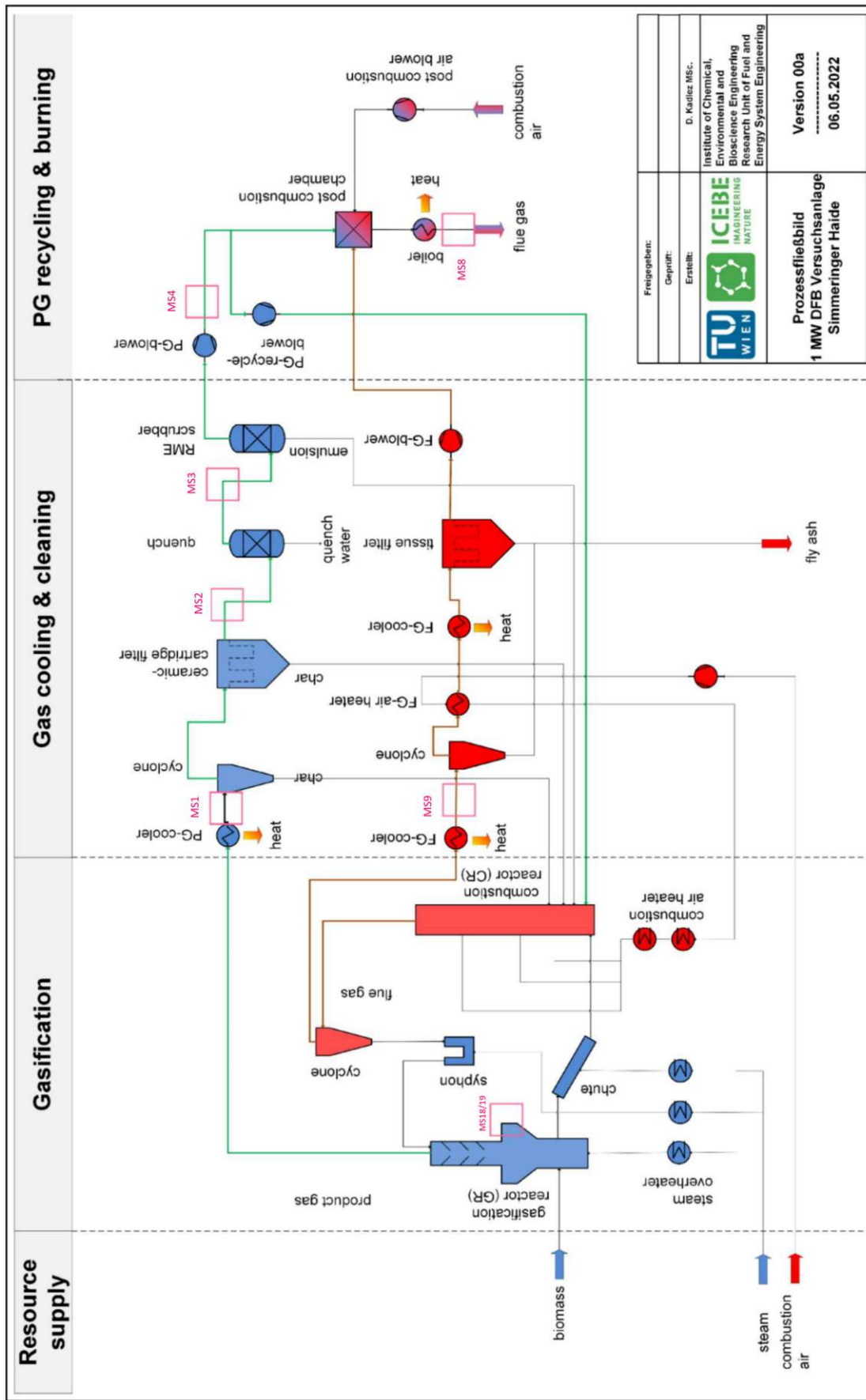


Figure 3.1: Process flow diagram with pink marked location of the measurement points[33]

## 3.4 Duration of commissioning

The commissioning of the 1MW DFB plant in Simmering continuously provided data such as temperatures, pressures, flow rates and gas compositions at the respective measuring points from 04.03.2022 to 17.03.2022. In order to make comparisons of DFB plants with similar construction, it is necessary to find a constant operating period. The main factors for comparison are the parameters of the gasification reactor and the gas composition. Figure 3.2 shows the temperature and pressure graph that occurred over the height of the upper and lower gasification reactor, as well as the gas composition after the product gas blower. In addition, the order of the measuring positions for temperature and pressure can be seen from the colored marking in the schematic diagram of the gasification reactor on the left side of the Figure. The exact height of the measuring locations can be taken from Figure 3.6.

Diagram a.) of Figure 3.2 shows the time graph of the temperatures in the gasification reactor during commissioning. First, it can be seen that the temperature at the bottom of the reactor (60\_TISA010) was 200°C lower at some points than the above located temperatures. Furthermore, it can be noticed that the temperatures at higher measuring points did not increase steadily. For example, the lower temperature in the bubbling zone (60\_TICSA020) was constantly higher than the upper temperature in the bubble zone (60\_TISA030). The temperature differences of the thermocouples in the countercurrent column (60\_TISA040-60\_TISA070) were permanently <40°C.

Diagram b.) of Figure 3.2 represents the time graph of the pressure difference to the ambient pressure in the gasification reactor during commissioning. At the bottom of the lower gasification reactor (60\_PISA010), a pressure jump with a peak of was measured on 09.03.2022. Furthermore, fluctuations were recorded on 10.03.2022, which amounted to a peak of 150mbar at the bottom of the gasification reactor. Pressure was permanently highest at reactor floor. The pressure measuring points positioned above were also influenced by significant pressure fluctuations, as it can be seen on 10.03.2022 at bubbling zone (60\_PIZA030). At constant operation, pressure in the measuring points of the countercurrent column remained low up to a maximum of 10mbar. At diagram c.) of Figure 3.2, the composition of the product gas after PG-blower over the period from 04.03.2022 to 17.03.2022 is shown. In Figure 3.1, the measurement point is marked with the MS4 designation. At points of oxygen absence there was gasification operation. First tries of gasification started on 07.03.2022 and 08.03.2022 with air as gasification agent. Steam gasification was tried for the first time in the afternoon of 09.03.2022 and 10.03.2022.



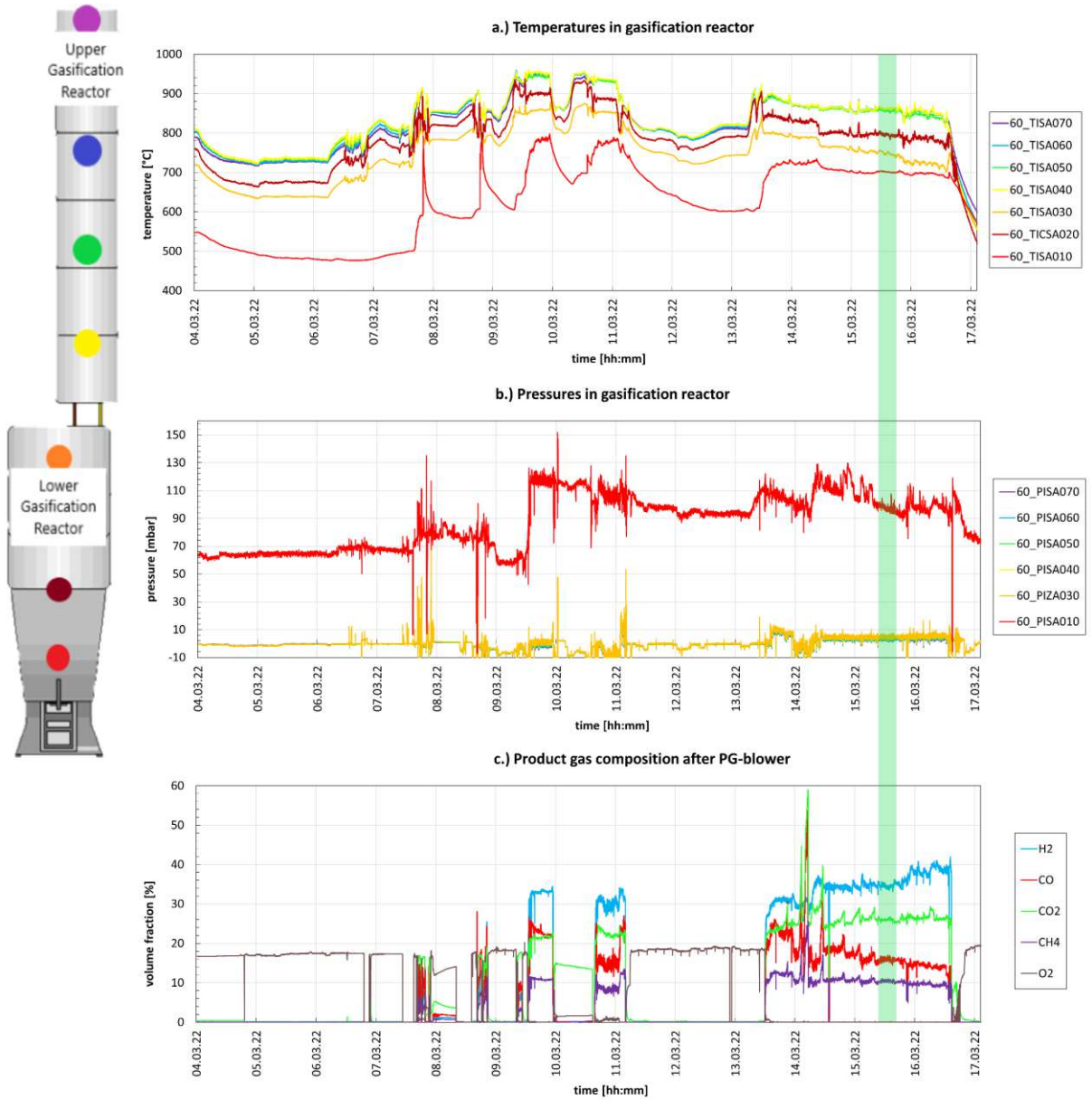


Figure 3.2: Course of a.) temperatures and b.) pressures in gasification reactor over height and c.) product gas composition during the entire gasification operation at commissioning from 04.03.2022 to 17.03.2022

Several hours of constant operation are required for evaluation. Beside multiple choices, the experimental period of 11:15-17:00 on 15.03.2022 was chosen. This period is marked green at Figure 3.2.

## 3.5 Data from 15.03.2022

For a more detailed view, the measured temperatures and pressures in gasification and combustion reactor from 11:15 to 17:00 on 15.03.2022 are shown in Figure 3.3 and Figure 3.4. On the left side of both Figures, the correct order of the measuring points is shown with the help of colored points in a schematic representation of the combustion reactor. The exact height of the measuring points can be read in Figure 3.6.

The upper diagram in Figure 3.3 shows the temperature profile in the gasification reactor. At this period, the temperature in countercurrent column (60\_TISA040 - 60\_TISA070) of gasification reactor was kept at about 850°C. As can be seen, the highest temperature in lower gasification reactor was reached in the middle of total height (60\_TISA020) with about 800°C. Top of lower gasification reactor (60\_TICSA030) remained at a temperature of about 760°C, while bed temperature (60\_TISA010) at about 700°C. All temperatures stayed constant during this period. Second chart in Figure 3.3 graphically represents the pressure difference to the ambient pressure over the same time period. Pressure at the reactor bed (60\_PISA010) was kept constant at 110 mbar between 11:45 to 15:52 and 16:20 to 17:00. Outside of these two periods, the pressure difference in bed increased abruptly to a maximum of 120 mbar. The pressure measurement points located in the countercurrent column were kept constant at about 5 mbar throughout this period.

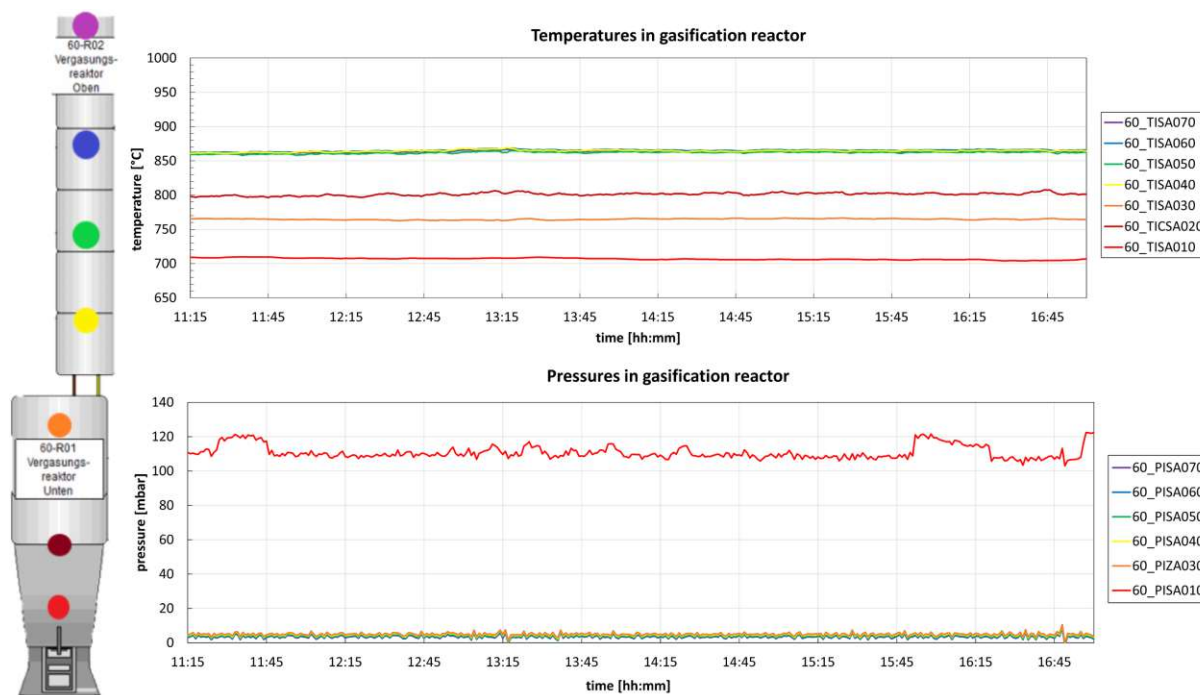


Figure 3.3: Temperature and pressure in gasification reactor on 15.03.2022 from 11:15 to 17:00

In addition, the temperatures and pressures of the combustion reactor were considered with the help of Figure 3.4.

The upper diagram, temperature in combustion reactor, shows four constant temperature profiles of originally five temperature measurement points in the combustion reactor. The highest temperature measurement point (61\_TISA050) was removed from diagram due to abrasive damage. The remaining temperature profiles stayed constant during the whole time period of 11:15 to 17:00. Its value was increasing with the height of the column and ranged from about 820°C to 880°C.

Measured pressure differences in combustion reactor are plotted over time in the diagram below. While the pressure fluctuated in the upper part of the combustion reactor in the range of -3 to 11 mbar, the lower two measuring points oscillated at an average of 128,1 mbar and 291,3 mbar, indicating a fluidized bed. In general, pressures were decreasing towards the top until a negative pressure was reached on top.

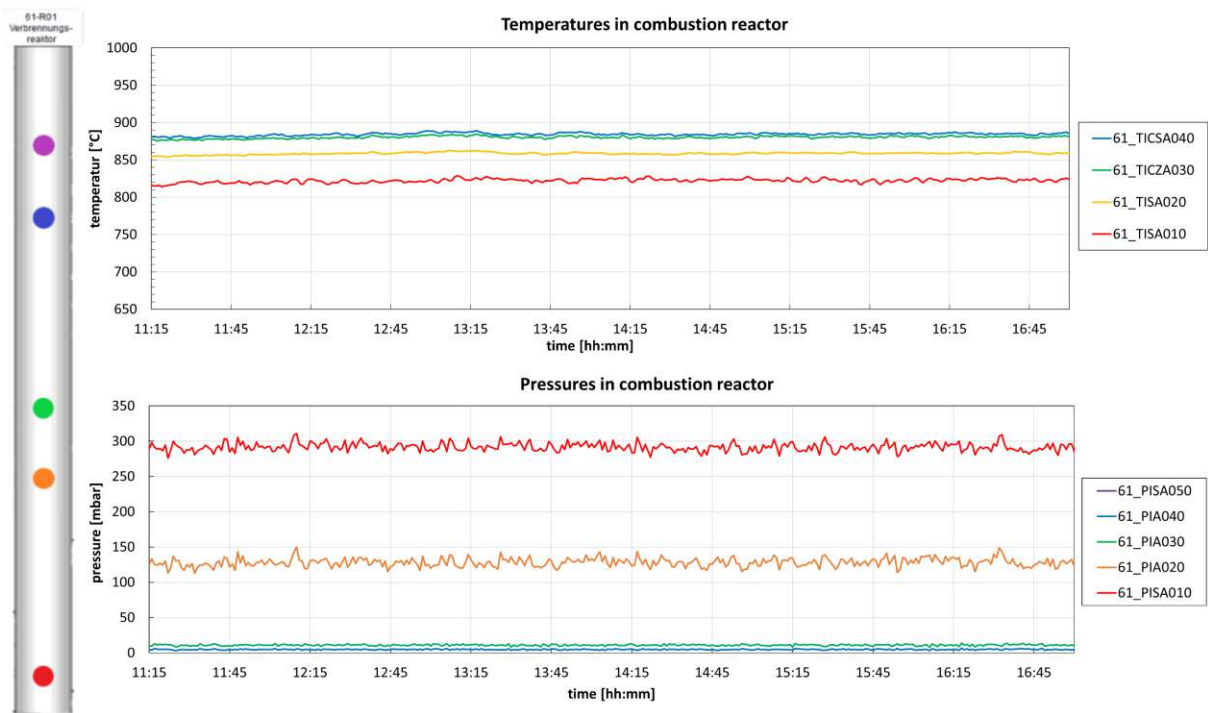


Figure 3.4: Temperature and pressure in combustion reactor on 15.03.2022 from 11:15 to 17:00

Product gas composition after product gas blower (79-G01) from 11:15 to 17:00 is plotted in Figure 3.5. The depicted measurement results are based on online measurements. Deviations in comparison to Table 3.8 can be attributed to differences in measurement time and methods.

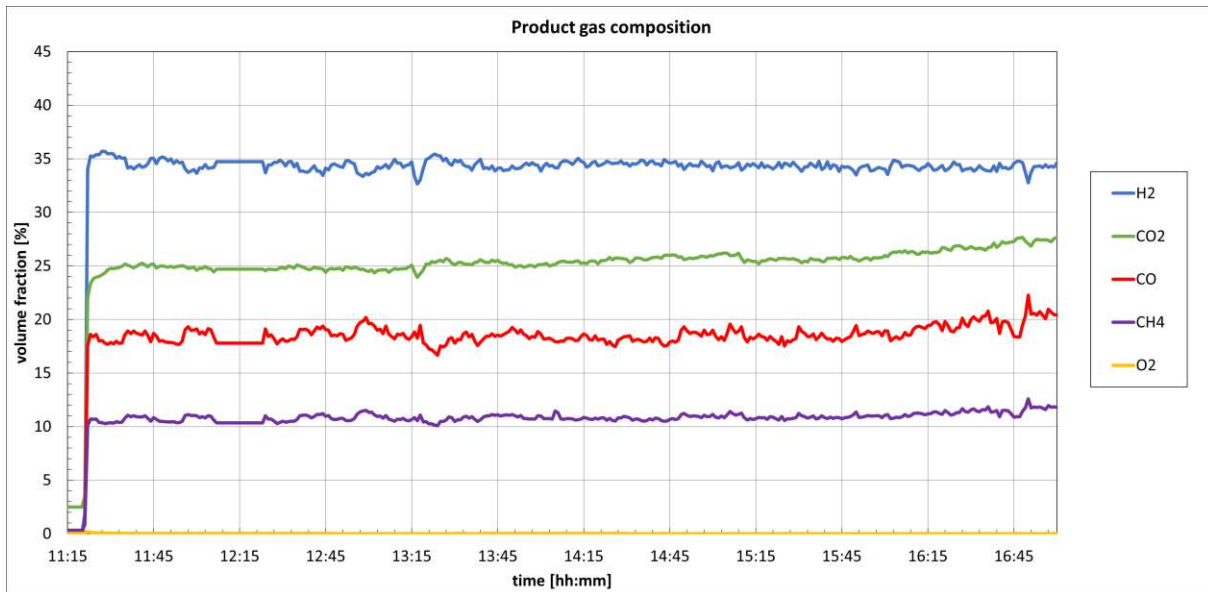


Figure 3.5: Product gas composition after product gas blower on 15.03.2022 from 11:15 to 17:00

### 3.6 Modifications and changes during 11:15 - 17:00

During operation, any changes of the control variables and malfunctions were recorded in the plant logbook. To gain an understanding of the operation and measurement changes associated with the variable changes, Table 3.5 lists the recordings made in the plant logbook during time period from 03:30 to 17:00. On purpose, entries before 11:15 on that day are also included in the following Table to be able to include possible influences.

### 3.7 Process flow diagram of reactors

In Figure 3.6, a schematic process flow diagram of the DFB reactor is given. All in- and outputs during the gasification operation and for preparation as bed material and wood pellets input are marked and labeled. Temperature and pressure measurement points are displayed. These measurement points show three data. As described in the legend, the upper value is the label of the measurement point. Data from chosen gasification period were averaged and listed at the second row. The last value of the legend gives an idea about the height of the measurement points. This value refers to the lowest measuring point of the combustion reactor, which is located at the bottom of the combustion reactor and represents the zero point.

### Changes and noticeable phenomena during operation

time [hh:mm]	entry
03:30	Addition of 151kg limestone done
07:00	Addition of another 150kg limestone done
09:12	Maintenance work at afterburner chamber leads to flow rate of 860Nm <sup>3</sup> /h of 110-G01
09:25	Heating oil decreased to 15%
09:29	Combustion air 2 valve (82-CV320) from 13% to 18%
09:30	Reactor air blower (82-G01) -2%
09:39	Product gas blower (79-G01) from 5 mbar to 3 mbar
09:41	High CO <sub>2</sub> content detected
09:45	Heating oil increase to 20
09:50	Incorrect MRU measurement (sum of the values high above 100%)
09:55	Fixing the MRU problem by air flushing
10:20	Sample gas taken at radiation cooler (MS1 at Figure 3.1)
10:26	Combustion air 2 valve (82-CV320) from 18% to 14%
10:28	Full load operation at 220 kg/h → 940kW (wrong calibration)
10:44	Tar measurement after radiation cooler (MS1 at Figure 3.1)
10:51	Bunker change
11:05	Gas sample taken after product gas filter
11:07	Fuel input increased from 220 kg/h to 230 kg/h
11:16	Gas sample taken after quench
11:36	Fuel input decreased from 230 kg/h to 227.5 kg/h
12:06	Filter change in MRU
12:20	MRU flushing
12:31	Measurement at product gas filter
13:39	Tar measurement between quench and RME scrubber
14:15	Bunker change
14:29	Gas sample taken after quench

Table 3.5: Logbook entries on commissioning day 15.03.2022

## 3.8 IPSEpro Simulation results

IPSEpro is an equation-oriented steady state simulation program for model implementation. Due to the complex structure in terms of the number of plant components, inputs and outputs, a sequentially modular solver would cause iteration problems. Further information about the operation scheme of IPSEpro can for example be read in the publication "Development and Application of a Simulation Tool for Biomass Gasification Based Processes" from T. Pröll (2008) [35]. An IPSEpro process flow diagram, as example, can be seen in the journal paper "Experimental development of sorption enhanced reforming by the use of an advanced gasification test plant" by S. Müller (2017)[36]. The input to the IPSEpro model, the recorded operation data, allows the program to simulate missing data. Energy and mass balances are used for this purpose,

which take the entire plant into account.[33]

As described in the simulation report of TU Wien, assumptions were made in the planning phase, which are reflected in present simulation results and are listed below:

- Heat exchangers and coolers are considered ideal lossless
- Nitrogen does not enter the system via any flushing entry, but only through one entry in the gasification reactor and another in the combustion reactor
- Temperature input values were rounded to whole numbers
- Due to inactive emulsion recycling, it is not considered in simulation
- During operation there was no bed material input and output

Figure 3.7 shows a sankey diagram of the gasification and combustion reactor with its energy in- and outputs. The diagram was created by TU Wien out of the simulation results from 15.03.2022 between 11:15 and 17:00.[33]

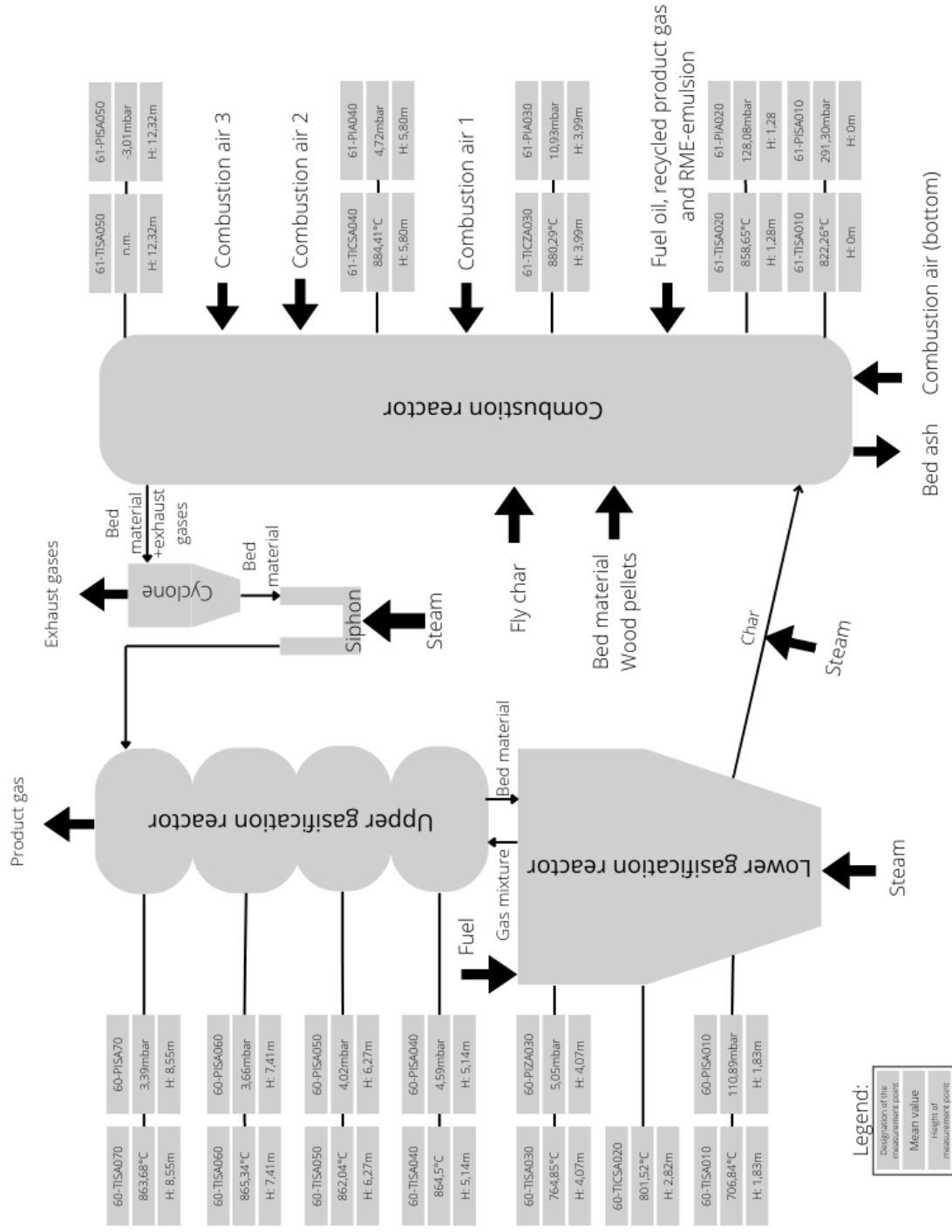


Figure 3.6: Designations, mean values and locations of the temperature and pressure measurement points at the gasification and combustion reactor

The gasification reactor has three material flow inlets and two material flow outlets. These are each connected to an energy supply or an energy removal. 580.2 kW of energy was supplied via the fuel (high grade wood chips analysis chapter 3.1). Steam with an energy of 23 kW entered the gasification reactor as gasification agent. The 211.1 kW net heat in the gasification reactor were supplied by bed material. Char with a thermal and chemical energy of 206,7 kW left the gasification reactor via the chute into the combustion reactor. On top of gasification reactor, 512 kW product gas, consisting of tar (chemical energy of 16.8 kW), char (chemical energy of 9.3 kW), gas itself (chemical energy of 378.8 kW) and its heat (thermal energy of 107.1 kW), was leaving the gasification process into cleaning section. As the gasification reactor, the combustion reactor has 3 material flow inputs and 2 material flow outlets. Beside char and bed material exchange with gasification reactor, heated combustion air with 82.5 kW was entering the CR. Additionally to char and heated air, auxiliary fuel (heating oil and recycled product gas) provided 237.9 kW of heating power. About 54 kW of this was provided by recycled product gas and the rest by extra light fuel oil. On top of the combustion reactor, flue gas with thermal power of 259.1 kW was leaving the combustion reactor into flue gas cleaning section. A balancing of the power inputs and outputs leads to the power loss in the respective reactor. This results in a heat loss of 95 kW in the gasification reactor and 63.3 kW in the combustion reactor.

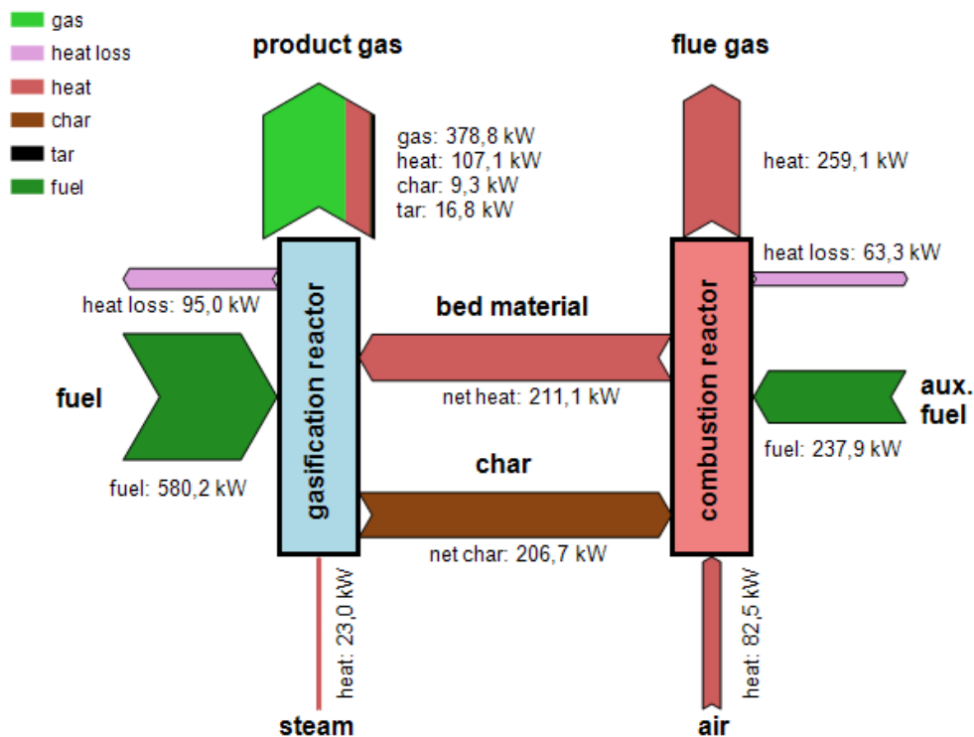


Figure 3.7: Energy in- and outputs during operation of 1MW DFB gasification plant in Simmering on 15.03.2022 between 11:15 to 17:00[33]



In addition to the power values in the sankey diagram, also performance indicating key figures resulted from the IPSEpro evaluation. These PIKFs are listed in Table 3.6. Mostly they are unitless operating ratios that make it easier to understand the operation at a certain moment and to make comparisons between other operating points and gasification plants. Compared in this table are typical values from literature, design values and results from the operating point in Simmering on 15.03.2022. Exact definitions and descriptions of each PIKF can be found in section 2.5. The PIKF determined by IPSEpro indicate a high content of gasification agent (steam) and combustion agent (combustion air) compared to expected values. In contrast, the water conversion rates, product gas yield and cold gas efficiency of the operating hours examined turn out to be very low.

Operation parameter	Unit	Typical values[37]	Design values	IPSE analysis
Relative water conversion rate	$\text{kg}_{\text{H}_2\text{O}}/\text{kg}_{\text{fuel,daf}}$	0.07 - 0.14	0.13	0.06
Absolute water conversion rate	$\text{kg}_{\text{H}_2\text{O}}/\text{kg}_{\text{H}_2\text{O}}$	0.09 - 0.16	0.17	0.06
Steam to fuel ratio	$\text{kg}_{\text{H}_2\text{O}}/\text{kg}_{\text{fuel,daf}}$	0.5 - 1	0.8	1.1
Logarithmic deviation from CO-Shift eq.	-	(-0.3) - (-0.5)	-0.23	-0.37
Cold gas efficiency gasification reactor	%	87 [38]	74.5	65.3
Overall cold gas efficiency gasification reactor	%	66-73 [18]	n.a.	49.5
Char combusted in combustion reactor	$\text{kg}_{\text{char}}/\text{kg}_{\text{fuel,daf}}$	n.a.	0.16	0.19
Air ratio combustion reactor	-	n.a.	1.37	1.57
Product gas yield	$\text{Nm}^3_{\text{db}}/\text{kg}_{\text{daf}}$	1.4 [6]	1.12	0.98

n.a. ... not available

Table 3.6: Performance indicating key figures of the data from 11:15-17:00, 15.03.2022[33]

### 3.9 Product gas composition at different measurement points

In addition to the online measurements after the product gas blower, further samples were taken offline in gas bags. Gas samples were taken by TU Wien at several points of the plant around 15.03.2022.[33] As marked in the process flow diagram Fig. 3.1, measurement points are located above the freeboard (MS18/19), after radiation cooler (MS1), after ceramic filter (MS2), after quench and thus before RME-scrubber (MS3) and after the PG-blower (MS4).

Table 3.7 indicates the measured components. Tar, dust, and water content was measured on each measurement point. NH<sub>3</sub>, H<sub>2</sub>S and HCl was only measured before and after ceramic filter.

<b>Component</b>	<b>Above freeboard</b> <i>MS18/19</i>	<b>After radiation cooler</b> <i>MS1</i>	<b>After ceramic filter</b> <i>MS2</i>	<b>After quench</b> <i>MS3</i>	<b>After PG-blower</b> <i>MS4</i>
Tar (gravimetric and GC/MS)	•	•	•	•	•
Dust	•	•	•	•	•
Water content	•	•	•	•	•
NH <sub>3</sub> , H <sub>2</sub> S, HCl	-	•	•	-	-

- ... measured
- ... not measured

Table 3.7: Measured product gas components on each DFB plant location

After product gas sampling on site, the tars and the inorganic components NH<sub>3</sub>, H<sub>2</sub>S and HCl were analysed in the laboratory of TU Wien. Tars were determined gravimetrically and by gas chromatograph-mass spectroscopy (GC/MS), NH<sub>3</sub> and HCl by ion chromatography (IC), and H<sub>2</sub>S by potentiometric titration. Additionally, organic compounds, water, dust and fly char content were analyzed. Table 3.8 shows the amount of each component at the respective measuring point. Many changes in product gas composition occurred at the countercurrent column. There was no sampling point directly after the countercurrent column. The next measuring point was after the radiation cooler. During countercurrent column and radiation cooler carbon monoxide decreased from 22.3% to 17.8%, while carbon dioxide increased from 17.1% to 23.4%. Between these measurement points, there was also minimal decomposition of hydrocarbon chains, oxygen,

hydrogen and carbonyl sulfide. Nitrogen and methane increased minimal. Except of a nitrogen increase, these components nearly stay constant at further sampling points. The water content dropped rapidly during the quenching process from 54% to <2% due to temperature decrease. Dust and fly char content decreased with the number of plant apparatuses flowed through. The inorganic component ammonia dropped rapidly after the quench (MS3), while hydrogen sulfide fluctuated. In comparison, hydrogen chloride was not present in all measurement locations. Since this work relates to performance during operation, the results of the tars are listed primarily for completeness. Tars with high molecular weight, which are collected via vacuum evaporation, are called gravimetric tars.[16] While the sum of tars without BTX (measured by GC/MS) decreased during the flow through the countercurrent column and the radiation cooler (comparison of MS18/MS19 and MS1), the BTX tars increased in the meantime. The next jump in tar composition was caused by the quench. Same procedure occurred, sum of tars without BTX decreased due to the water spray cooling (MS3), and the BTX tars increased in the meantime. The next measuring point was after the product gas blower (MS4), whereby product gas already passed RME-scrubber, and resulted in a decrease of the sum of tars.

## 3.10 Ashfraction analysis

At operation start, the plan was to collect ashes after several apparatuses of the two purification sections to see where which ash contents are separated. Due to time and logistical problems, the ashes were only taken from the designated collection points. Normally, at DFB gasification plant in Simmering, four different types of ashes are collected at two different locations.

### 3.10.1 First ash sampling point

Bed ash is removed from the lowest point of the CR. Via a cooling screw (61-H04) and 2 further screws (61-H05, 61-H06), bed ash is transported to bed ash bin (61-B03), where test samples can be collected. Bed ash is a mixture of olivine and calcite (bed material), hydrocarbon chains (unburned char), secondary- and trace elements, which wood contains. Since no unusual results were expected, bed ash was not analyzed.

### 3.10.2 Second ash sampling point

Exhaust gas from the CR flows through several cleaning and cooling apparatuses. Including radiation cooler (80-K01, 80-K02), cyclone (81-C01) and the fabric filter (84-F01). At these three points, fly ash was deducted and transported to the flow bin via two transport screws (81-H01, 84-H04) and a cooling screw (84-H02). Mainly expected were inorganic components. Results are given below in Table 3.9. The sum of the inorganic components in the table results in 62.36%, the remaining 37.64% is occupied by oxygen. Especially magnesium (20.64 wt.-%), silicon (10.5 wt.-%), calcium (22.14 wt.-%) and iron (5.14 wt.-%) show high values. Potassium and total organic carbon content is with 1.3 wt.-% and <0.5 wt.-% low.

Color		light brown
Consistency		solid
Mg	[wt.-%]	20.64
Si	[wt.-%]	10.5
Ca	[wt.-%]	22.14
Fe	[wt.-%]	5.14
K	[wt.-%]	1.3
S	[wt.-%]	0.14
Cr	[wt.-%]	0.77
P	[wt.-%]	0.27
Ni	[wt.-%]	0.19
Al	[wt.-%]	0.26
Mn	[wt.-%]	0.1
Cl	[wt.-%]	0.11
Co	[wt.-%]	0.03
Zn	[wt.-%]	0.02
Ba	[wt.-%]	0.17
Cu	[wt.-%]	0.04
Sr	[wt.-%]	0.04
Ti	[wt.-%]	-
TOC*	[wt.-%]	<0.5

\*Total organic carbon

Table 3.9: Fly ash analysis from sampling taken on 16.03.2022 analyzed by TU Wien[33]

Component	Unit	Above freeboard	After radiation cooler	After ceramic filter	After quench	After PG-blower
		10:30 MS18/19	10:20 MS1	11:05 MS2	14:25 MS3	10:06 MS4
CO <sub>2</sub>	[%]	17.1	23.4	23.8	23.9	23.4
C <sub>2</sub> H <sub>4</sub>	[%]	2.8	2.4	2.2	2.3	2.3
C <sub>2</sub> H <sub>6</sub>	[%]	0.4	0.2	0.2	0.1	0.2
O <sub>2</sub>	[%]	0.4	0.1	0.1	0.2	0.0
N <sub>2</sub>	[%]	5.3	6.2	8.6	8.2	8.3
CH <sub>4</sub>	[%]	9.4	10.1	9.6	10.0	9.9
CO	[%]	22.3	17.8	16.4	16.9	17.5
H <sub>2</sub>	[%]	42.2	39.9	39.0	38.3	38.5
COS	ppm	0.2	0.0	0.0	0.0	0.0
Water content	[Vol.-%]	51	56	54	<2	<2
Dust content	[g/Nm <sup>3</sup> ]	21.79	0.03	n.d.	n.d.	n.d.
Fly char content	[g/Nm <sup>3</sup> ]	9.10	2.13	1.75	n.d.	n.d.

#### Inorganic components

H <sub>2</sub> S	ppm	-	93	-	60	82
NH <sub>3</sub>	ppm	-	915	-	4	4
HCl	ppm	-	<1	-	<1	<1

#### Tars

Tar gravimetric	[g/Nm <sup>3</sup> ]	5.57	4.57	3.56	0.55	0.34
Tar sum GC/MS without BTX	[g/Nm <sup>3</sup> ]	10.76	7.16	7.73	0.92	0.20
Tar sum GC/MS BTX	[g/Nm <sup>3</sup> ]	21.50	29.88	29.54	38.92	37.34
Benzene	[g/Nm <sup>3</sup> ]	>8.9	>8.9	>8.9	>8.9	>8.9
Toluene	[g/Nm <sup>3</sup> ]	4.4	1.1	1.3	1.1	0.4
Xylene	[g/Nm <sup>3</sup> ]	1.7	0.4	0.4	0.4	0.1
Tar sum GC/MS Total	[g/Nm <sup>3</sup> ]	32.26	37.04	37.27	39.84	37.53

n.d. ... not detected

- ... not measured

Table 3.8: Product gas composition on different measurement points on 15.03.2022[33]



## Chapter 4

---

# Discussion

---

In the following sections, results are evaluated, anomalies in data are interpreted and occurred mechanisms are explained. The topics described in section 1.2, Aim of the work, are discussed, and further anomalies are clarified.

### 4.1 Comparison of wood chips and typical wood pellets

Table 3.1 lists data of fuel content of commissioning used wood chips and typical wood pellets. According to the standard DIN EN ISO 17225-4:2014-06, high-grade wood chips need to have a water content  $\leq 25$  wt.-% (category A1). For the use of wood pellets for industrial purposes, DIN EN ISO 17225-2:2021-09 must be considered, in which a water content  $\leq 10$  wt.-% and a waterfree ash content  $\leq 0.7$  wt.-% (category A1) is specified. Thus, with regard to the water and ash content, the requirements are achieved and are typical for the respective fuel. The remaining values are related to dry basis and therefore well comparable without noticeable deviations from each other. Only the ash content of wood chips with 0.89 wt.-%<sub>db</sub> deviates slightly from the wood pellets with 0.2 wt.-%<sub>db</sub>, resulting in a higher ash output from the reactors. This is due to an increased content of bark in the wood chips. In addition, increased contact with the soil and forest residue could contribute to a higher ash content.

The comparison of x-ray fluorescence analysis of the two fuel ashes in Table 3.2 shows no decisive differences between commissioning used wood chips and typical wood pellets. The interaction of potassium and silicon lowers the ash melting temperatures and can lead to the formation of bridges and subsequently clog pipes, for example.[27] The measured ash melting characteristics in Table

3.3 lists temperatures high above 1000°C. Since the maximum temperature in the combustion reactor was reached at about 950°C, there is no risk of agglomeration. The composition of the ash has an influence on the reactions that take place in the gasification reactor during operation. Reason for this is the use of the bed material olivine. Olivine is a magnesium iron silicate and has no extraordinary effect when it is freshly used for the first time. The activation of olivine by the elements contained in the ash, such as calcium and potassium, generate positive effects during gasification. As mentioned by A. Larsson et al. 2021, both fuels show typical compositions.[5] Further information about the impact of ash composition to ash melting point were described by D. Boström et al. 2012.[39] The bed material olivine is activated after about 5 hours of operation. For the selected time window of the evaluation, a partial activation of the bed material can be assumed. The activation of the limestone contained in the mixture is already completed after a few hours. Thus, according to Table 3.5, the 300kg of limestone added a few hours earlier were already activated.

## **4.2 Analyzing the chosen constant operation point on 15.03.2022 from 11:15 to 17:00**

As it can be seen on Figure 3.2 Diagram c.) Product gas composition after PG-blower, the DFB plant was not in permanent gasification mode from 04.03. to 17.03. On days like 06.03. for example, the diagram only shows a PG composition of 19% oxygen, since no nitrogen and noble gases are measured. Short-time steam gasification operation was started on afternoon of 09.03. and 10.03. for example, whereby already remarkable compositions of up to 35% hydrogen were achieved. During 13.03. and 17.03., the plant operated in gasification mode. On 15.03. from 11:15 to 17:00, a constant gasification progress was held with more than 24 hours of lead time. Another deciding reason for choosing this period are the measurement samplings, which are made within this time frame. The respective measurement point is marked in Figure 3.1. Table 3.7 lists the measured components on each location.

Temperature as well as pressure and PG composition remained approximately constant in gasification reactor from 11:15 to 17:00, as Figure 3.3 depicts.



## 4.2.1 Analyzing temperature profile of GR between 11:15 to 17:00

The lower GR measures temperature on three different measurement points, distributed over the height. Figure 3.6 shows a schematic design of GR and CR with the online measurement points and its mean values during 11:15 and 17:00. Due to only a few fluctuations in the temperatures during the period under consideration, the mean temperatures provide a good basis for discussion. At the bottom temperature measuring point 60\_TISA010 the lowest temperature was measured with about 707°C. Due to the high temperature difference to the next measuring point, it can be assumed that this sensor is located in area of the fluidized bed on the bottom of gasification reactor. The steam entered the GR with a temperature of 425°C, causing the bed material, located at the bottom of the GR, to cool slightly.

The middle temperature measurement point (60\_TICSA020, splash zone) of the lower gasification reactor measured a temperature of 802°C on average. The temperature measurement above (60\_TISA030, freeboard) showed an average of 765°C. The temperature measured at the bottom of the upper GR (60\_TISA040) fluctuates around 865°C. This can be explained with the help of fuel entry. Wood chips enter the GR at atmospheric temperature via an on-bed feeding system and is held partly in the region between splash zone and freeboard by buoyancy. Volatile gases are released from the fuel, which is associated with an endothermic reaction. Due to this reaction, the bed material cools downwards and the temperature drop of the bed material between upper GR and lower GR can be explained. As the char is mixed with bed material to enter the combustion reactor via the chute, the volatile gases rise. In the freeboard, the volatile gases increasingly come into contact with the hot bed material. The mixture of the hot bed material and the still colder volatile gases represented a mixture with an average temperature of 765°C (60\_TISA030).

There are four temperature measuring points in the upper gasification reactor. These four mean temperatures varied only slightly from each other between 865°C and 862°C. Small variations result from the minimally different insertion depths of the temperature sensors.

## 4.2.2 Analyzing pressure profile of GR between 11:15 to 17:00

The lower diagram in Figure 3.3 shows the pressure profile in gasification reactor from 11:15 to 17:00.

The lowest pressure measuring point is located in the with steam fluidized bed (60\_TISA010), which resulted in a high pressure difference to the ambient pressure of 111 mbar on average.

In the considered period, 2 pressure jumps at this measuring point could be detected. Each pressure jump, at 11:20 and 15:50, increased the pressure to a pressure difference to the ambient pressure of about 120mbar. According to the plant log at Table 3.5, an increase in fuel input from 220 kg/h to 230 kg/h occurred at 11:07. At 11:36, the fuel input was decreased from 230 kg/h to 227,5 kg/h. Increasing the fuel input counteracts the buoyancy of steam and volatile gases and results in a higher pressure. Conversely, reducing the fuel input would again lead to a pressure loss, which according to 11:45 also occurred. Increasing pressure at 11:20 a.m. and decreasing pressure at 11:45 a.m. were influenced by change in fuel input with a delay of some minutes. Log book entries stop at 14:29, so another fuel input change at around 15:50 was not documented. Since the fuel input was changed only once, the second pressure increase cannot be caused by the fuel input. Furthermore, an increase in fuel input would tend to bring a pressure increase in the upper pressure measuring points, which was not noticeable. Earlier, adjustments of 82-CV320 were noted. This valve is responsible for the control of hot air 2 and offers the possibility to adjust bed material circulation. At 10:26, the valve position was reduced from 18% to 14%, which may result in a higher bed material input to the gasification reactor at the settings used. A change of the trim at the air input in the combustion reactor can lead to a higher bed material level in the bubbling bed with a time delay, which increases the pressure loss at the bottom of GR. Further adjustments in hot air 2 input were not noted at the log book between 11:15 and 17:00 on 15.03.2022.

Except of bed pressure loss in fluidized bed at the bottom of lower gasification reactor (60\_PISA010), the remaining pressure measuring points (60\_PIZA030 - 60\_PISA070) showed a low pressure of about 3 to 5 mbar on average. These pressure measurement points were unaffected by the change of hot air trimming and fuel input.

### **4.2.3 Analyzing temperature profile of CR between 11:15 to 17:00**

Figure 3.4 depicts the measured temperature and pressure losses in combustion reactor between 11:15 and 17:00. Both diagrams, temperature and pressure loss, show no noticeable abnormalities.

Temperature was increasing with the height of the measurement point. Three combustion air inputs effect a complete combustion. Combustion is an exothermic reaction, which resulted in a temperature increase from bottom to top. The highest temperature measuring lance was damaged by abrasion of bed material and detected no temperatures.

The lower diagram of Figure 3.4 shows the pressure of five measuring sensors divided over the height of the CR. At the bottom of the combustion reactor, the pressure loss of 291 mbar (61\_PISA010) was more than twice as high as at the bottom of the gasification reactor. The pressure measuring point above (61\_PIA020) still recorded a pressure of 128 mbar. Both pressure measurements indicate a high bed in the combustion reactor. The pressures of the upper part of the combustion reactor were decreasing, until finally the top pressure measuring point showed a negative pressure loss. This is due to the afterburner chamber blower, which ensures the flow of exhaust gases through the exhaust gas cleaning section.

## 4.3 Evaluation of the performance indicating key figures

In section 2.5, formulas of different performance indicating key figures (PIKF) are shown. These PIKF are used for a quick overview of the whole operation process, or for comparison of different modes of operation. Table 3.6 shows the results of some of these described parameters. The following subsections discuss each PIKF and theorize regarding its amount. Each is followed by an assessment of whether the respective PIKF is suitable for comparison with other operations.

### 4.3.1 Evaluation of water conversion rate

A differentiation is made between relative and absolute water conversion. The relative water conversion refers its consumed water to the converted dry and ash free fuel. Absolute water conversion relates its consumed water to the supplied water. According to design values and typical values mentioned additionally in Table 3.6, the gasification operation of 15.03. from 11:15 to 17:00 deviated significantly from these values.

Main reason for the deviation from design values are due to the lower temperatures in the gasification reactor. In the lower/upper gasification reactor, the average temperature over time and reactor height was 758/864°C during the test period. Higher temperatures in the range of 810/930°C on average would enhance the emission of volatile gases from the fuel, decomposition of the tars and the water gas shift reaction. A. Aghaalikhani et al. generated a DFB biomass gasification model in ASPEN plus for process optimization.[40] According to the model developed in this research, the hydrogen content in the product gas increases from 35% at 725°C to 45% at 830°C. To a large extent, this is due to the water gas shift reaction, which is slightly exothermic

and thermodynamically more reactive at high temperatures. Thus, the lower temperature is responsible for lower water conversion, relatively and absolutely.

Due to partial load operation, the H<sub>2</sub>O supply was higher than originally intended for the amount of fuel supplied. This results in a high steam to fuel ratio of 1.1 kg<sub>H<sub>2</sub>O</sub>/kg<sub>fuel,waf</sub>. This can be attributed to the fact that the DFB gasification plant constructed in Simmering is designed for almost double the capacity as it was operated during commissioning. The larger cross-section of the gasification reactor means that a certain mass flow of steam is required for fluidization, which must not be undercut even with a lower fuel feed. A higher water conversion results in higher cold gas efficiency, as less excess steam needs to be heated electrically before feeding. It also means that less water and steam have to be heated to gasification temperature in the gasification reactor, which would reduce the additional fuel/heating oil feed in the combustion reactor.

#### 4.3.2 Evaluation of logarithmic deviation from CO-Shift eq.

Table 3.6 lists additionally the logarithmic deviation from CO-Shift eq.. As described at equation 2.6, this value shows how close operation is to water-gas shift reaction equilibrium. Is the value <0, so composition is on side of reactants. Is logarithmic deviation from CO-Shift eq. =0, so equilibrium is reached. Values >0 can not be thermodynamically achieved by water gas shift reaction. The interaction of devolatilization, other gasification reactions such as water-gas reaction or steam and dry reforming, and of the varying water content in the product gas leads to a balance change to the side of the products H<sub>2</sub> and CO<sub>2</sub>. For example, high steam input to the gasification reactor shifts the reaction equilibrium more to side of the reactants ( $p\delta_{eq.CO-shift} < 0$ ), because of a higher steam content in the product gas.[23] However, due to water separation by quenching, this effect is significantly reduced.

Another reason for the occurred logarithmic deviation from CO-Shift eq.  $p\delta_{eq.CO-shift}$  are low temperatures in GR. A temperature raise in the gasification reactor from 750°C to 850°C can change  $p\delta_{eq.CO-shift}$  from -0.4 to -0.05.[40]

#### 4.3.3 Evaluation of product gas yield

Table 3.6 also lists PGY. Compared to the design value (1.12 Nm<sup>3</sup><sub>db</sub>/kg<sub>waf</sub>), the calculated PGY from 15.03.2022 (0.98 Nm<sup>3</sup><sub>db</sub>/kg<sub>waf</sub>) was lower than expected. Reason for the lower yield was once again due to the bad implementation of part-load operation. As described in upper

subsections 4.3.1 and 4.3.2, excessive performance deviation from the design layout, without making adjustments to the fluidization, will result in ineffective water conversion.

#### 4.3.4 Evaluation of cold gas efficiency

A distinction is made between the cold gas efficiency (equation 2.7) and the overall cold gas efficiency of the entire DFB system (equation 2.8). Cold gas efficiency  $\eta_{CG}$  is the ratio of the power contained in the product gas to the power of the fuel provided in percentage. Overall cold gas efficiency  $\eta_{CG,o}$  additionally considers the fuel which is fed to the combustion reactor and heat losses.

Cold gas efficiency connects the product gas yield with lower heating value of the product gas, and thus indirectly product gas composition. PGY did not reach the design value. According to other authors, obtained lower heating value with 12.15 MJ/Nm<sup>3</sup> was comparatively average.[7, 36] So the estimated and desired cold gas efficiency of 74.5% would be reached, if product gas yield would be higher. During commissioning, a cold gas efficiency of about 65% was reached.

The overall cold gas efficiency depends to a great extent on the heat losses. Normally, heat losses of a plant decrease with increasing power size. S. Kern et al. calculated heat losses of about 17-20% of the input power at 100kW DFB gasification plant. In the experiment described by S. Kern, however, it was the old DFB design of TU Wien, which, for example, did not yet have a countercurrent column.[23] Test runs at the advanced DFB steam gasification plant at TU Wien showed higher heat losses than the previous design. For example, in a paper from A. M. Mauerhofer et al., published in 2018, test runs at advanced 100kW plant of TU Wien with soft wood and comparable bed material (90% olivine and 10% limestone) showed heat losses of about 28%.[26] Commissioning of 1MW DFB plant in Simmering demonstrated similar heat losses with 27%. In relation to the 10-fold plant size, heat losses were expected to be lower than in the pilot plant of the TU Wien. But, as pilot plant of TU Wien, demonstration plant in Simmering is also constructed for research purposes. However, due to many nitrogen flushed measuring points of the DFB system and additionally of the two gas cleaning sections, heat losses increase and explain the similar values. According to S. Kern et al in 2013[23], using the heat radiation losses calculated by M. Stidl[41] for the 10MW DFB steam gasification plant in Oberwart, industrial scale plants can be estimated to have a heat loss of 2% of the input fuel power.

### 4.3.5 Evaluation of char combusted in combustion chamber

Despite a low fuel input of 135 kg/h instead of 234 kg/h for full load, more char per kg fuel as designed was burnt in the combustion chamber. Thus, more char was transferred to the combustion reactor via the chute than was intended in the design layout. This is due to the low average temperature of 707°C in the lower gasification reactor. The char to combustion reactor can be decreased by varying the temperature in lower gasification reactor. At lower GR pyrolysis of biomass takes place. Lower pyrolysis temperatures showed minimally decreased higher heating values of char in previous research due to carbon enrichment, but significantly higher char yields.[42, 43] Generating more char in lower GR results in a higher char input to the CR via the chute. By varying the temperature in the lower gasification reactor, a good balance can thus be achieved between the formation of volatile gases and char. In case of commissioning, the gasification reactor was operated at too low temperatures, which favored char production. Thus, less volatile gases emitted and this resulted in a lower PGY.

### 4.3.6 Evaluation of air ratio in combustion reactor

According to the results shown in Table 3.6, air ratio in combustion reactor was higher than required. For a complete burning of char and additional fuels, a combustion air ratio of  $\lambda = 1.37$  was required. Higher combustion air ratios resulted in additional air that had to be heated. This decreases the efficiency. However, moderate higher combustion air ratios are welcome, thus exhaust gas composition has to fulfill its requirements all the time. A combustion air ratio  $\lambda > 1.37$ , as it was the case in the discussed periode with  $\lambda = 1.57$ , compensates for possible CO peaks.

### 4.3.7 Helpful PIKF for comparison

The **relative water conversion rate** relates the water consumed in the gasification reactor via water gas, water gas shift, and steam reforming reactions to the fuel input. The fuel was softwood chips with common chemical composition as often used in publications. Therefore, a comparison at higher fuel inputs and higher temperature levels is useful to assess the effects on the process. The equation relates the consumed water to the water, that is introduced into the process. Since only 58% of the designed input power was fed to the GR, but fluidization needed to maintain, steam input into the system was higher than necessary and this resulted in a lower **absolute**

**water conversion rate.** Furthermore, this resulted in lower temperatures in GR. Therefore, this PIKF is not an ideal benchmark.

Thus, due to incorrectly part load operation, and therefore the high steam input and low GR temperatures, **logarithmic deviation from CO shift eq.** of -0.37 was higher compared to design value of -0.23.[23, 40] A correct fuel input, equivalent to 1MW fuel power, and higher temperatures in gasification reactor enhance this PIKF. Higher fuel input favors the addition of char to the combustion reactor, minimizing the addition of fuel oil and increasing the temperature in the GR. Thus, a comparison to the effects of correct part and full load operations on the logarithmic deviation from CO shift eq. would be interesting.

The situation is similar with the **product gas yield.** This is significantly influenced by the water gas shift reaction and tar cracking. Higher temperatures in the GR would release more volatile gases from the fuel and thus increase product gas yield.

**Cold gas efficiency** is suitable for comparison with industrial-scale plants. The reason for this is that it neglects heat losses, which decrease with growing plant size in power. With increasing product gas yield and high product gas quality, the cold gas efficiency is enhanced.

The **overall cold gas efficiency** reflects the interaction of various process-decisive parameters. These include increased temperatures in the GR, improved hold up, heat losses, the increase of fuel input and all the associated consequences. This PIKF is well suited for an in-plant comparison of the DFB gasification plant in Simmering to test the knowledge obtained during commissioning.

The **char combusted in the combustion chamber** is already of less value when evaluating the data. However, the amount of char burned during operation is important. The temperature in the lower gasification reactor serves as an indicator.

**Air ratio in combustion reactor** should be kept within a certain range. Hot air enters the combustion reactor at a temperature of about 400°C and thus has a cooling effect on the 900°C hot reactor atmosphere. To keep the combustion efficiency high and still obtain sufficient combustion, a combustion air ratio of 1.3 to 1.5 should be maintained.

Table 4.1 provides an overview of the PIKFs discussed in this subsection including their symbols and units.

Symbol	Performance indicating key figure	Unit
$X_{H_2O,rel}$	relative water conversion rate	$\left[ \frac{kg_{H_2O}}{kg_{fuel,daf}} \right]$
$X_{H_2O,abs}$	absolute water conversion rate	$\left[ \frac{kg_{H_2O}}{kg_{H_2O}} \right]$
$p\delta_{eq.CO-shift}$	logarithmic deviation from CO shift eq.	[-]
PGY	product gas yield	$\left[ \frac{Nm^3_{PG}}{kg_{fuel,daf}} \right]$
$\eta_{CG}$	cold gas efficiency	[%]
$\eta_{CG,o}$	overall cold gas efficiency	[%]
-	char combusted in combustion reactor	$\left[ \frac{kg_{char}}{kg_{fuel,waf}} \right]$
$\lambda$	air ratio in combustion reactor	[-]

Table 4.1: List of the useful PIKF including their symbol and unit

## 4.4 Evaluation of product gas composition

The product gas composition significantly influences the lower heating value and thus the cold gas efficiency. As part of the work to evaluate the performance of the 1MW demonstration plant in Simmering, this section focuses primarily on the basic product gas composition. Further research will focus on the conversion of the tars, which are listed here mainly for the sake of completeness.

### 4.4.1 Evaluation of CO, CO<sub>2</sub>, H<sub>2</sub> and CH<sub>4</sub> contents

The results of product gas composition at different plant locations are presented in Table 3.8. In the countercurrent column, CO decreased, whereas CO<sub>2</sub> increased. In a publication, A. M. Mauerhofer et al. describes the change of product gas composition along the countercurrent column height of 100kW DFB gasification plant of TU Wien.[16] These experiments showed similar results as mentioned above. Differences arise when analyzing the hydrogen content. While the hydrogen content decreased slightly during commissioning, tests at the TU Wien showed an increasing H<sub>2</sub> content over the height of countercurrent column. In the experiments of A. M. Mauerhofer et al in 2019, the influence of temperature and bed material over the height of the countercurrent column was investigated. It was found that high temperatures over the height



of the countercurrent column contribute more to water and tar conversion than catalytically active bed materials.[16]

Furthermore, large differences can be seen when looking at the pressure loss across the countercurrent column, which is depicted in Figure 4.1. The schematic depiction of the gasification reactor on the left in Fig. 4.1 is out of scale and for understanding purposes only. Figure 4.2 depicts the pressure profile of bed material tests performed at TU Wien by A. M. Mauerhofer et al. in 2019.[16] Thereby, 50/50 mixtures of olivine and limestone or feldspar and limestone, as well as 100% quartz were tested as bed materials. The reason for the comparison of the DFB steam gasification plants, which differ in performance, are years of experience of TU Wien in fluidized bed gasification and the high conversion rate especially in the referred test. In the comparison of the pressure losses discussed in the following, the average pressure values of the bed materials, tested by A. M. Mauerhofer et al., are always used. The pressure loss in the bottom of the bubbling bed of the two experiments considered is comparable at about 112mbar. Especially the constrictions in the countercurrent column offer potential. Pressure losses of more than 2mbar per constriction stage can be achieved by high bed material circulation, as shown in this experiment. This resulted in a total pressure loss of about 9mbar over a height of about 2.5m (4 constrictions) at the 100kW countercurrent column located at TU Wien. In comparison, a pressure loss of 2mbar on average was achieved over a height of about 3.5m (5 constrictions) of the countercurrent column during commissioning at 1MW DFB plant in Simmering. A high pressure loss is a sign of enhanced gas-solid contact, which increases the conversion rate.[16] Table 4.2 compares main product gas components of commissioning in Simmering with values from tests at TU Wien, both at partial load operation.[44] Hydrogen, methane and the water content deviate slightly in comparison. Significant deviations at CO and CO<sub>2</sub> content indicate oxygen input into the gasification reactor. This is possible in case of insufficient chute fluidization.

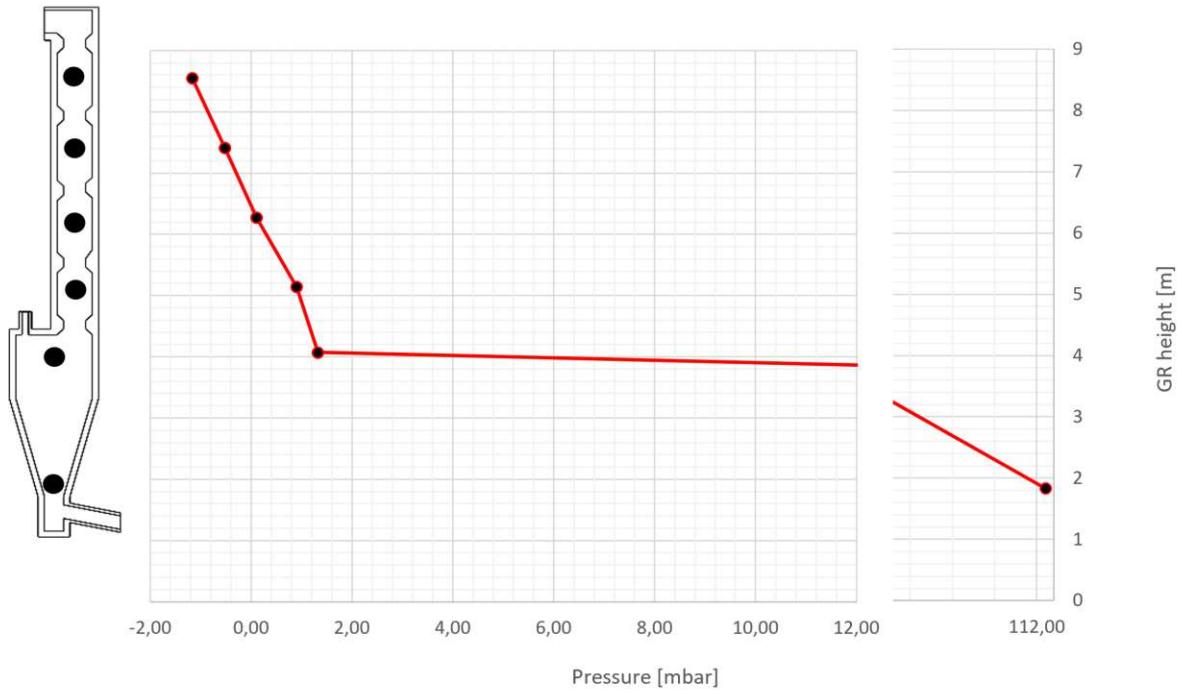


Figure 4.1: Average pressure profile over height of gasification reactor from 15.03.2022 between 11:15 to 17:00 at 1MW DFB steam gasification plant in Simmering

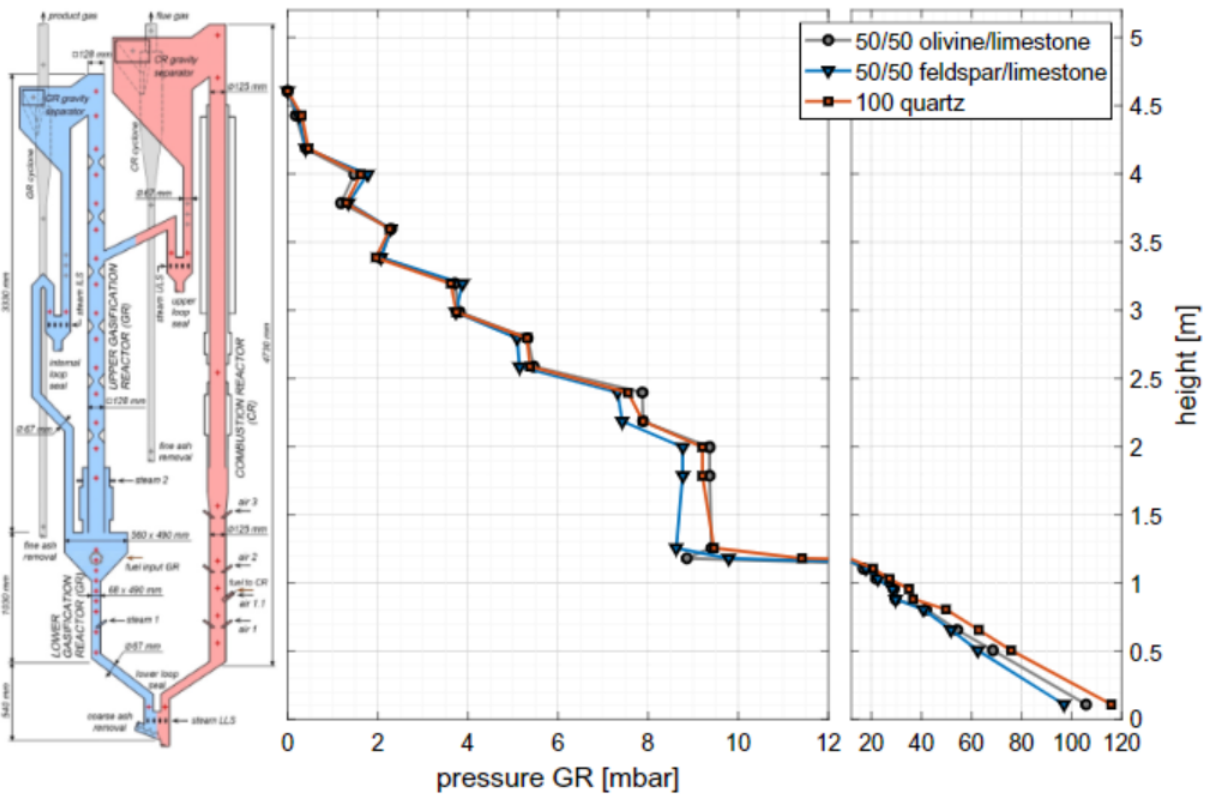


Figure 4.2: Average pressure profile over height of gasification reactor from bed material tests at 100kW DFB steam gasification plant of TU Wien evaluated by A. M. Mauerhofer et al. in 2019[16]

Component	Unit	Simmering (1MW)	TU Wien (100kW)
Fuel input	[%]	58	47
H <sub>2</sub>	[vol.-% <sub>db</sub> ]	35.9	38.2
CO	[vol.-% <sub>db</sub> ]	18.4	23.8
CO <sub>2</sub>	[vol.-% <sub>db</sub> ]	24.19	21.1
CH <sub>4</sub>	[vol.-% <sub>db</sub> ]	10.8	9.5
Water content	[vol.-%]	56	57

Table 4.2: Comparison of product gas composition after gasifier between 1MW DFB plant in Simmering and 100kW DFB plant at TU Wien at partial load operation[44]

#### 4.4.2 Evaluation of dust, fly char and water content

Non-reactive dust and parts of fly char were separated in cyclone, which explains the decrease of both components between MS18/19 and MS1, as listed in section 3.8. The water content dropped to <2 vol.% after quenching as the still present steam cools rapidly and thus condenses.

#### 4.4.3 Evaluation of NH<sub>3</sub> content

Nitrogen content (N<sub>2</sub>) was partially slightly increasing with proceeding measuring location, due to the nitrogen flushed online measurement points and inspection glasses. A low nitrogen content of 0.14 wt.-%<sub>db</sub> was measured in commissioning used wood chips. Thus no nitrogenous air was used for gasification, the fuel nitrogen is the only nitrogen that can be found in product gas, as long as chute fluidization with steam was sufficient. In 2013, V. Wilk et al. researched the conversion of nitrogen in the fuel in gasification reactor.[45] Therein the release of the nitrogen in the fuel at temperatures >300°C is described. Most of the nitrogen is present as ammonia (NH<sub>3</sub>). Furthermore, lower amounts of N<sub>2</sub>, HCN and nitrogen in tars and chars are produced. After ceramic filter and quench, ammonia content dropped from 915 ppm to 4 ppm. Analysis of quench water shows ammonia contents of 862 mg/l. Since there is no reason for NH<sub>3</sub> to separate from product gas in ceramic filter and in view of the quench water analysis, it can be said, that

ammonia is separated in quench. The addition of water in the quench cools the product gas and water comes into contact with ammonia. This causes the ammonia to dissolve in the liquid phase and ammonium ions are produced. The equilibrium between ammonia and ammonium shifts to the side of the ammonium as the temperature and pH decrease. This would explain the reduction of ammonia in the product gas during the quenching process.[46, 47] Examination of the subsequent RME fluid showed about half of the  $\text{NH}_3$  (484 mg/l) contained in the quench water. As nitrogen content in fuel is low, no problems in cleaning section were expected. Fuels with higher nitrogen content, as waste wood, were tested by V. Wilk et al. in Güssing, where an RME scrubber was sufficient for the separation of ammonia.[45, 48]

#### 4.4.4 Evaluation of $\text{H}_2\text{S}$ content

The  $\text{H}_2\text{S}$  measurement results of the various measuring points MS1, MS3 and MS4 are listed in Table 3.8. Reason for fluctuations of the values could be system adjustments that were made within the 4 hours between the measurements. The sulfur content of the wood chips is  $<0.02$  wt.%, which compares well with other research. COS which was still present in small amounts in the lower gasification reactor at MS18/19 was no longer detected after the radiation cooler. Reason for this could be the conversion to  $\text{H}_2\text{S}$  (eq. 6.10) in the countercurrent column. J. Hongrapipat et al. discussed  $\text{H}_2\text{S}$  and  $\text{NH}_3$  generation in product gas of a DFB gasification system in 2016.[48] Various influencing factors such as temperature, steam to fuel ratio, bed material and residence time are investigated in relation to  $\text{H}_2\text{S}$  generation. It was noticed that more  $\text{H}_2\text{S}$  is formed with increasing gasification temperature. At low temperatures, the sulfur remains in char or metal sulfides are formed.[48, 49] The metals are present in bed material, which means that less  $\text{H}_2\text{S}$  is formed when the bed material is catalytically active, such as olivine and limestone in our case. At temperatures above  $400^\circ\text{C}$ , instead of metal sulfides, such as  $\text{FeS}$ ,  $\text{ZnS}$ , etc., more  $\text{H}_2\text{S}$  is formed.[48, 50] Likewise, an increasing steam to fuel ratio leads to a higher  $\text{H}_2\text{S}$  content in the product gas. The residence time showed only minor effects in these experiments.[48] In our case, steam to fuel ratio of  $1.1 \text{ kg}_{\text{H}_2\text{O}}/\text{kg}_{\text{fuel,daf}}$  promoted the low  $\text{H}_2\text{S}$  formation during gasification, which explains the presence after the radiation cooler. In product gas cleaning section of the 1MW DFB steam gasification plant in Simmering, there is no unit for sulfur removal, such as absorption by caustic soda, chemical by iron salts, or adsorption by activated carbon.[51] Fluctuations, which occurred at the individual measuring points, can be

explained by operating activities, which may have occurred within the 3.5 hours between the measurements, in this value range.

## 4.5 Further anomalies that occurred during evaluation periode

To show the effects of part-load operation on fluidization visually, the operating and design values were plotted in a Grace diagram in Figure 4.3 by TU Wien.[33] In both, the combustion reactor and the two gasification reactors, the respective design parameters were not achieved. The design parameters would ideally be achieved by full-load operation. In the Grace diagram, both axes,  $U^*$  (Eq. 6.13) and  $d_p^*$ (Eq. 6.14), are plotted in logarithmic scale. According to the Geldart classification, the bed material is categorized in the lower range of the AB group. Thus, it is suitable for fast fluidization and yet the operation of a bubbling fluidized bed is possible.[19] Differences between full and partial load arise in the dimensionless superficial gas velocity  $U^*$ . In all three reactors, the value was lower than design velocity. The empty pipe velocity is decisive for this. To increase this velocity in the lower and upper gasification reactors, a higher fuel or steam input is required. Since the steam input was already set to 1 MW fuel input, the steam to fuel ratio of  $1.1 \text{ kgH}_2\text{O/kg}_{\text{fuel}}$  was high anyway. Thus, in this case, only an increased fuel input would remain to reliably operate the upper gasification reactor as a turbulent fluidized bed. This would release more volatile gases, which would flow upward through the upper GR and increase pipe velocity. Due to the logarithmic scale, the deviation from full load should also not be underestimated in the combustion reactor. In order to operate this reliably as a circulating fluidized bed, there is the possibility of an increased combustion air input. Since the combustion air ratio  $\lambda = 1.57$  is already high here, the char input, and thus the fuel input into the lower gasification reactor, should be increased.

## 4.6 Future DFB gasification in Simmering

In this section, reference is made to processes and parameters in order to obtain as many and useful data sets as possible from the future campaigns of the 1MW DFB steam gasification plant in Simmering.

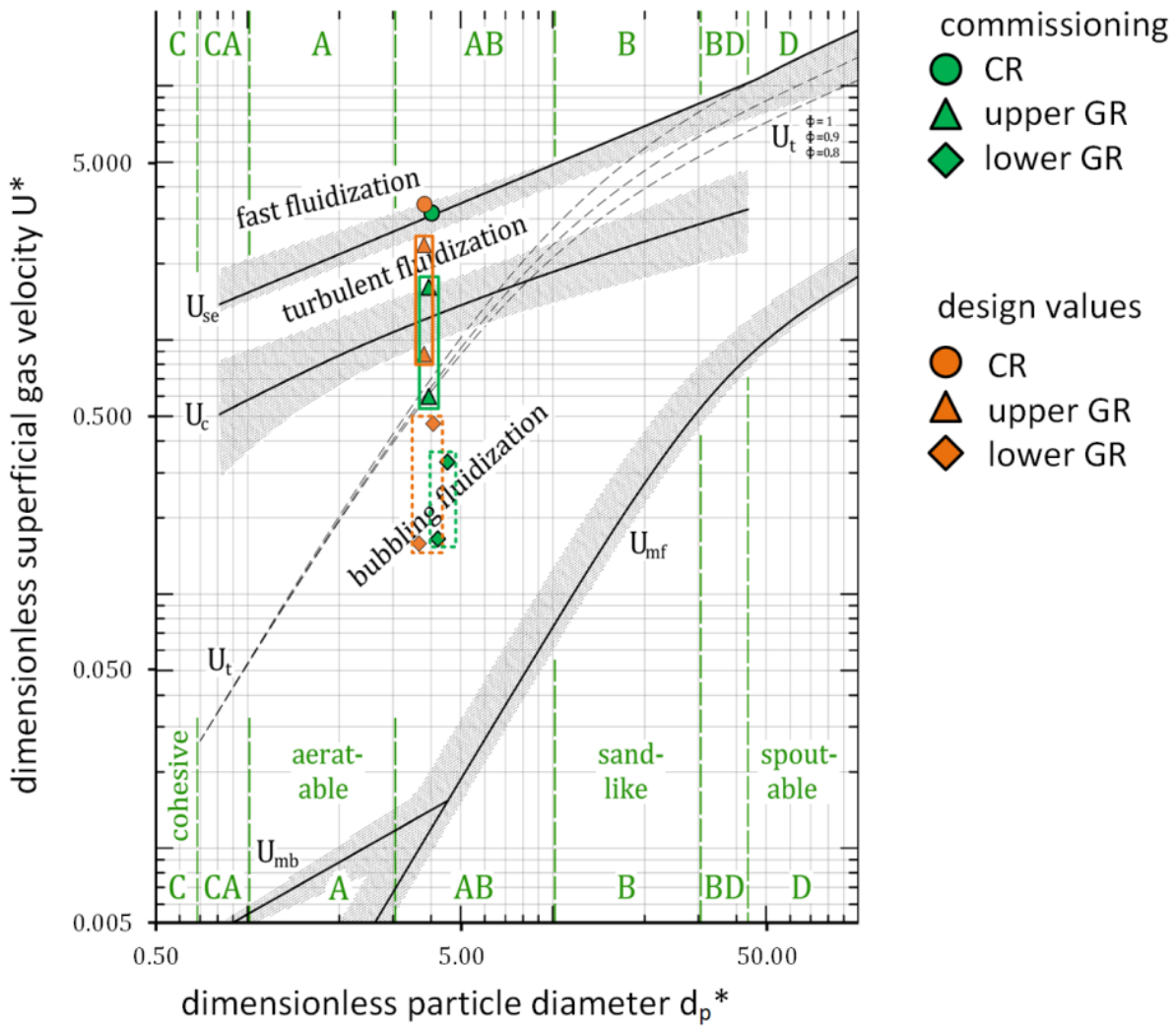


Figure 4.3: Comparison of the fluidization of design values and commissioning used values[33]

### 4.6.1 Reliable calibration of the fuel dosing screws

The crucial problem during commissioning operation of the new DFB gasification plant in Simmering was the incorrect fuel supply. Wrong calibration led to less fuel input into the GR. This resulted in releasing less volatile gases and lower conversion rates due to high steam to fuel ratio in GR. To avoid this problem in the future, a reliable and consistent calibration method is necessary.

For more accurate calibration results, the operating time should be increased during the calibration process. Ideally, the run-up time should also be increased after a certain screw drive power has been set on the motor. For commissioning, the transport of the calibrated material from first floor of the plant was done by human physical force. This limited the operating time and thus the accuracy. For higher accuracy, the transport from the 3rd floor of the plant should be done

directly downwards and the obtained weight should be recorded there.

## 4.6.2 Indicative values for a promising operation

A steam to fuel ratio can be calculated preliminary. In case of using softwood chips, a steam to fuel ratio of about  $0.7 \text{ kg}_{\text{H}_2\text{O}}/\text{kg}_{\text{fuel,daf}}$  should be aimed at. Higher steam to fuel ratios do not have a decisive influence on the gas composition, but lead to increased energy consumption.[44, 52] If other fuels are used, a steam to carbon ratio should be preferred for comparison instead. In order to utilize the full potential of the countercurrent column, an eye should be kept on the holdup. Commissioning measured values are noted in Figure 3.6. Figure 4.1 and Figure 4.2 compare pressure profiles of commissioning in Simmering at 1MW plant and at 100kW plant at TU Wien. Higher circulation values result in higher pressure loss and thus in enhanced gas-solid contact. Indicative values are about 110mbar at bottom of GR and total pressure loss of about 8mbar over height of countercurrent column. As the pressure loss in the countercurrent column, the temperature in the gasification reactor should be about  $60^\circ\text{C}$  higher than during commissioning. Guide values for this are  $770^\circ\text{C}$  in the lower gasification reactor (averaged value of all three temperature measuring points),  $930^\circ\text{C}$  in the upper gasification reactor and about  $950^\circ\text{C}$  at the outlet of the combustion reactor.

## 4.6.3 Correct part load operation

Fuel shortage or excess power of the product gas, as was the case according to Kraussler et al. 2016 at 8,5MW DFB gasification plant in Oberwart[29], can demand a desirable partial load operation. A WGS pilot plant was operated for 2250 h with the product gas from the DFB steam gasification plant. More detailed information on this partial load operation of the DFB plant is provided in the diploma thesis by M. Binder on the Fe/Cr-based WGS catalyst used.[53] According to this, no significant changes in the product gas or tar production were achieved after 100 hours of partial load operation of the DFB gasifier with constant settings as steam input. Also the temperatures were kept constant by automatic regulation.

M. Kolbitsch reports in his dissertation 2016 about fuel input tests, comparing fast changes to 47kW and 92kW fuel input at the 100kW DFB gasifier of TU Wien.[44] In this case, an effort was also made to keep the parameters constant by increasing auxiliary fuel and maintaining the steam inlet at the same value. The product gas composition showed no significant deviations compared to full load operation. Partial load operation was maintained for only 70 minutes in

this test.

Based on the publications mentioned above, it can thus be said that the steam-to-fuel ratio at part load operation has no negative influence on the product gas composition. Thus, the significant lower temperature profile affected the limited conversion rates during part-load operation of the commissioning of the 1MW DFB steam gasification plant in Simmering.[29, 53, 44]

Correct part-load operation consists of the accurate interaction of fuel input, steam supply and bed material circulation. Steam input should be adjusted according to a steam to fuel ratio to maintain a bubbling bed in the lower GR and turbulent fluidization in the upper GR, but still be limited in the high range due to decreasing efficiency. Chute fluidization should be active to prevent the combustion air from entering the gasification reactor. A reference value for pressure loss of 60-PISA010 on bottom of the lower GR is between 90-120mbar, depending on bed material mass in the system. A pressure loss of 8mbar over height of upper GR should be regulated. The bed material circulation should be adjusted by regulating the three combustion air inputs in the combustion reactor to achieve a sufficiently high temperature in the GR. Approximately 840°C at the 60-TICSA020 temperature measurement point (in the center of the lower GR, splash zone) will ensure that sufficient volatile gases can escape from the fuel and yet an appropriate amount of char is carried into the combustion reactor. This keeps the addition of fuel oil to the combustion reactor moderate. The upper GR should have as high temperatures as possible, up to 960°C.



## Chapter 5

---

# Conclusion and Outlook

---

DFB steam gasification is a promising way to produce medium calorific gas from various fuels e.g. wood chips, bark and residual waste. The complex gas purification process implemented in Simmering provides an ideal basis for further processing the obtained product gas into more valuable fuels and chemicals.

Commissioning in Simmering was completed with wood chips for practical reasons. In addition to problems, including leaking heaters and hardened limestone, an incorrect dosing screw calibration, in particular, caused operating difficulties. Performance indicating key figures suffered from low fuel input, which consequently resulted in high steam to fuel ratios and low temperatures. 100 kW DFB steam gasification plant of TU Wien, in comparison, was able to achieve a higher product gas yield and thus higher cold gas efficiencies due to higher temperatures in the gasification reactor during part load operation. The decisive factors for these results were higher temperatures, higher bed material circulation, and active chute fluidization in comparison to the commissioning of the 1 MW DFB plant in Simmering. Main product gas composition did not deviate significantly from comparable gasification processes at 100kW DFB plant at TU Wien. During future full and part load gasification operation in Simmering, temperatures of about 850/920°C (lower/upper) should be maintained in gasification reactor. Pressure loss over the countercurrent column can be increased to 10 mbar. Steam to fuel ratio should be lower with values about  $0.8 \text{ kg}_{\text{H}_2\text{O}}/\text{kg}_{\text{fuel,daf}}$  and lower to enhance cold gas efficiency and still provide sufficient fluidization of the gasification reactor. After evaluation of the initial commissioning results, further system optimization can be made in future research. Fuel tests are necessary to ensure sustainability and economic viability in further scale-up. The efficiency of the gas cleaning section has to be evaluated. At the same time, investigations regarding the pollution cycles in the system due to RME, fly ash and emulsion recirculation are appropriate.



Die approbierte gedruckte Originalversion dieser Diplomarbeit ist an der TU Wien Bibliothek verfügbar  
The approved original version of this thesis is available in print at TU Wien Bibliothek.

## Chapter 6

---

# Notation

---

### 6.1 Chemical reactions

Water gas reaction:



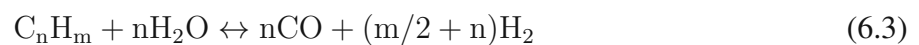
$$\Delta H_{R,25^\circ\text{C}} = +131,3 \text{ kJ/mol}[54]$$

Boudouard reaction:



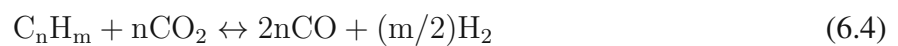
$$\Delta H_{R,25^\circ\text{C}} = +172,4 \text{ kJ/mol}[54]$$

Steam reforming:



$$\Delta H_{R,25^\circ\text{C}} = +206,2 \text{ kJ/mol}[54]$$

Dry reforming:



$$\Delta H_{R,25^\circ\text{C}} = +247,3 \text{ kJ/mol}[55]$$

Water-gas-shift reaction:



$$\Delta H_{R,25^{\circ}\text{C}} = -41,2 \text{ kJ/mol}[54]$$

Hydrogenation of carbon:



$$\Delta H_{R,25^{\circ}\text{C}} = -74,9 \text{ kJ/mol}[54]$$

Methanation:



$$\Delta H_{R,25^{\circ}\text{C}} = -206 \text{ kJ/mol}[56]$$

Complete oxidation:



$$\Delta H_{R,25^{\circ}\text{C}} = -393,4 \text{ kJ/mol}[54]$$

Partial oxidation:



$$\Delta H_{R,25^{\circ}\text{C}} = -110,5 \text{ kJ/mol}[54]$$

Carbonyl sulfide conversion:



$$\Delta H_{R,25^{\circ}\text{C}} = -34,6 \text{ kJ/mol}[29]$$

Archimedes number:

$$Ar = \frac{\rho_g(\rho_p - \rho_g)gd_p^3}{\mu_g^2} \quad [19] \quad (6.11)$$

Particle Reynolds number:

$$Re_p = \frac{d_p u \rho_g}{\mu_g} \quad [19] \quad (6.12)$$

Dimensionless velocity:

$$U^* = \frac{Re_p}{Ar^{\frac{1}{3}}} \quad [19] \quad (6.13)$$

Dimensionless particle diameter:

$$d_p^* = Ar^{\frac{1}{3}} \quad [19] \quad (6.14)$$

## 6.2 Symbols

Symbol	Meaning	Unit
$\dot{m}$	mass flow rate	$[\frac{kg}{s}]$
$\dot{V}$	volume flow rate	$[\frac{m^3}{s}]$
$p$	pressure	[Pa]
$p_i$	partial pressure	[Pa]
$v_i$	mass fraction in the fuel	[-]
$T$	temperature	[K]
$LHV_{PG}$	lower heating value of product gas	[MJ/m <sup>3</sup> ]
$LHV_{fuel}$	lower heating value of fuel	[MJ/kg]
$\dot{Q}_{loss}$	heat loss	[kW]
$\eta_{CG}$	cold gas efficiency	[-]
$\eta_{CG,o}$	overall cold gas efficiency	[-]
$K_{p,CO-shift}$	equilibrium constant of water gas shift reaction	[-]
$PGY$	product gas yield	$[\frac{Nm^3_{PG}}{kg_{fuel,daf}}]$
$\Phi_{SF}$	steam to fuel ratio	$[\frac{kg_{H_2O}}{kg_{fuel,daf}}]$
$\Phi_{SC}$	steam to carbon ratio	$[\frac{kg_{H_2O}}{kg_C}]$
$\Delta H_R$	enthalpy of reaction	[kJ/mol]
$Ar$	Archimedes number	[-]
$\rho_g$	gas density	[kg/m <sup>3</sup> ]
$\rho_p$	particle density	[kg/m <sup>3</sup> ]
$g$	gravitational acceleration	[m/s <sup>2</sup> ]
$dp$	particle diameter	[m]
$\mu_g$	gas viscosity	[kg/m s]
$Re_p$	particle Reynolds number	[-]
$u$	empty pipe velocity	[m/s]

## 6.3 Abbreviations

<b>Abbreviation</b>	<b>Meaning</b>
PG	product gas
GR	gasification reactor
CR	combustion reactor
daf	dry and ash free
H <sub>2</sub> O	water
C	carbon
CO	carbon monoxide
CO <sub>2</sub>	carbon dioxide
C <sub>n</sub> H <sub>m</sub>	hydrocarbon
PIKF	performance indicating key figures

---

# List of Figures

---

1.1	Global surface temperatures relative to 1880-1920 based on GISTEMP data, which employs GHCN.v3 for meteorological stations, NOAA ERSST.v4 for sea surface temperature, and Antarctic research station data[4] . . . . .	2
1.2	Basic principle of the DFB steam gasification process[6] . . . . .	3
2.1	Enhanced principle of the DFB steam gasification process[16] . . . . .	6
2.2	1 MW DFB steam gasification plant in Simmering with project name Waste2Value by BEST-research[21] . . . . .	10
2.3	Overview Piping and Instrumentation Diagram (PID) of 1MW DFB plant in Simmering	11
2.4	Measured permanent gas composition of the product gas[23] . . . . .	13
2.5	Total and specific gas production[23] . . . . .	13
2.6	Heating-up scheme . . . . .	16
2.7	Correct and incorrect fuel input comparison with respect to motor frequency . . . .	23
3.1	Process flow diagram with pink marked location of the measurement points[33] .	29
3.2	Course of a.) temperatures and b.) pressures in gasification reactor over height and c.) product gas composition during the entire gasification operation at commissioning from 04.03.2022 to 17.03.2022 . . . . .	31
3.3	Temperature and pressure in gasification reactor on 15.03.2022 from 11:15 to 17:00	32
3.4	Temperature and pressure in combustion reactor on 15.03.2022 from 11:15 to 17:00	33
3.5	Product gas composition after product gas blower on 15.03.2022 from 11:15 to 17:00	34
3.6	Designations, mean values and locations of the temperature and pressure measurement points at the gasification and combustion reactor . . . . .	37

3.7	Energy in- and outputs during operation of 1MW DFB gasification plant in Simmering on 15.03.2022 between 11:15 to 17:00[33] . . . . .	38
4.1	Average pressure profile over height of gasification reactor from 15.03.2022 between 11:15 to 17:00 at 1MW DFB steam gasification plant in Simmering . . . . .	56
4.2	Average pressure profile over height of gasification reactor from bed material tests at 100kW DFB steam gasification plant of TU Wien evaluated by A. M. Mauerhofer et al. in 2019[16] . . . . .	56
4.3	Comparison of the fluidization of design values and commissioning used values[33]	60



---

# List of Tables

---

2.1	Comparison of the DFB gasification plant design of different locations . . . . .	15
2.2	Heating-up rate . . . . .	17
3.1	Elemental analysis of A. commissioning used high grade wood chips and B. typical wood pellets[33, 32] . . . . .	26
3.2	RFA from A. high grade wood chips used at commissioning and B. typical wood pellets[33, 32] . . . . .	26
3.3	Analysis of ash melting characteristic of high grade wood chips made by fuel laboratory of TU Wien, released on 01.02.2022 and typical wood pellets analyzed by J.I. Arranz in 2015, COM2[33, 34] . . . . .	27
3.4	Average compositions of olivine and limestone with exemplary illustration aside[18, 33]	28
3.5	Logbook entries on commissioning day 15.03.2022 . . . . .	35
3.6	Performance indicating key figures of the data from 11:15-17:00, 15.03.2022[33] .	39
3.7	Measured product gas components on each DFB plant location . . . . .	40
3.9	Fly ash analysis from sampling taken on 16.03.2022 analyzed by TU Wien[33] . .	42
3.8	Product gas composition on different measurement points on 15.03.2022[33] . . . .	43
4.1	List of the useful PIKF including their symbol and unit . . . . .	54
4.2	Comparison of product gas composition after gasifier between 1MW DFB plant in Simmering and 100kW DFB plant at TU Wien at partial load operation[44] . . . .	57



Die approbierte gedruckte Originalversion dieser Diplomarbeit ist an der TU Wien Bibliothek verfügbar  
The approved original version of this thesis is available in print at TU Wien Bibliothek.

---

# Bibliography

---

- [1] C. A. Horowitz, “Paris Agreement,” *International Legal Materials*, vol. 55, pp. 740–755, 8 2016.
- [2] C. P. Morice, J. J. Kennedy, N. A. Rayner, P. D. Jones, C. . Morice, J. J. Kennedy, N. A. Rayner, and P. D. Jones, “Quantifying uncertainties in global and regional temperature change using an ensemble of observational estimates: The HadCRUT4 data set,” *Journal of Geophysical Research: Atmospheres*, vol. 117, p. 8101, 4 2012.
- [3] F. Kogan and W. Guo, “Strong 2015–2016 El Niño and implication to global ecosystems from space data,” <http://dx.doi.org/10.1080/01431161.2016.1259679>, vol. 38, pp. 161–178, 1 2016.
- [4] J. Hansen, M. Sato, R. Ruedy, G. A. Schmidt, K. Lo, and A. Persin, “Global Temperature in 2016,” 2017.
- [5] A. Larsson, M. Kuba, T. Berdugo Vilches, M. Seemann, H. Hofbauer, and H. Thunman, “Steam gasification of biomass – Typical gas quality and operational strategies derived from industrial-scale plants,” *Fuel Processing Technology*, vol. 212, 2 2021.
- [6] F. Benedikt, J. C. Schmid, J. Fuchs, A. M. Mauerhofer, S. Müller, and H. Hofbauer, “Fuel flexible gasification with an advanced 100kW dual fluidized bed steam gasification pilot plant,” *Energy*, vol. 164, pp. 329–343, 12 2018.
- [7] F. Benedikt, J. Fuchs, J. C. Schmid, S. Müller, and H. Hofbauer, “Advanced dual fluidized bed steam gasification of wood and lignite with calcite as bed material,” *Korean Journal of Chemical Engineering* 2017 34:9, vol. 34, pp. 2548–2558, 7 2017.

- [8] A. M. Mauerhofer, S. Müller, F. Benedikt, J. Fuchs, A. Bartik, and H. Hofbauer, “CO<sub>2</sub> gasification of biogenic fuels in a dual fluidized bed reactor system,” *Biomass Conversion and Biorefinery*, vol. 11, pp. 1101–1116, 8 2021.
- [9] S. Koppatz, C. Pfeifer, and H. Hofbauer, “Comparison of the performance behaviour of silica sand and olivine in a dual fluidised bed reactor system for steam gasification of biomass at pilot plant scale,” *Chemical Engineering Journal*, vol. 175, pp. 468–483, 11 2011.
- [10] T. Vilches, M. Seemann, and H. Thunman, “Influence of In-Bed Catalysis by Ash-Coated Olivine on Tar Formation in Steam Gasification of Biomass,” *Energy and Fuels*, vol. 32, pp. 9592–9604, 9 2018.
- [11] C. Pfeifer, S. Koppatz, and H. Hofbauer, “Steam gasification of various feedstocks at a dual fluidised bed gasifier: Impacts of operation conditions and bed materials,” 2011.
- [12] A. P. Steynberg, “Introduction to Fischer-Tropsch Technology,” *Studies in Surface Science and Catalysis*, vol. 152, pp. 1–63, 1 2004.
- [13] S. Pissot, R. Faust, P. Aonsamang, T. Berdugo Vilches, J. Maric, H. Thunman, P. Knutsson, and M. Seemann, “Development of Oxygen Transport Properties by Olivine and Feldspar in Industrial-Scale Dual Fluidized Bed Gasification of Woody Biomass,” *ACS Publications*, vol. 35, pp. 9424–9436, 6 2021.
- [14] J. Corella, J. M. Toledo, and G. Molina, “A Review on Dual Fluidized-Bed Biomass Gasifiers,” 2007.
- [15] S. Koppatz, J. C. Schmid, C. Pfeifer, and H. Hofbauer, “The Effect of Bed Particle Inventories with Different Particle Sizes in a Dual Fluidized Bed Pilot Plant for Biomass Steam Gasification,” *Industrial and Engineering Chemistry Research*, vol. 51, pp. 10492–10502, 8 2012.
- [16] A. M. Mauerhofer, J. C. Schmid, F. Benedikt, J. Fuchs, S. Müller, and H. Hofbauer, “Dual fluidized bed steam gasification: Change of product gas quality along the reactor height,” *Energy*, vol. 173, pp. 1256–1272, 4 2019.

- [17] K. Fuersatz, J. Fuchs, F. Benedikt, M. Kuba, and H. Hofbauer, “Effect of biomass fuel ash and bed material on the product gas composition in DFB steam gasification,” *Energy*, vol. 219, p. 119650, 3 2021.
- [18] A. M. Mauerhofer, S. Müller, A. Bartik, F. Benedikt, J. Fuchs, M. Hammerschmid, and H. Hofbauer, “Conversion of CO<sub>2</sub> during the DFB biomass gasification process,” *Biomass Conversion and Biorefinery*, vol. 11, pp. 15–27, 2 2021.
- [19] J. C. Schmid, C. Pfeifer, H. Kitzler, T. Pröll, and H. Hofbauer, “A new dual fluidized bed gasifier design for improved in situ conversion of hydrocarbons,” *ICPS conference*, 2011.
- [20] F. Kirnbauer and H. Hofbauer, “The mechanism of bed material coating in dual fluidized bed biomass steam gasification plants and its impact on plant optimization,” *Powder Technology*, vol. 245, pp. 94–104, 9 2013.
- [21] M. Kuba and G. Weber, “COMET-Forschungsprojekt Waste2Value,” 2022.
- [22] P. Kaushal, “Modelling of the fast fluidized combustion reactor of a dual fluidized bed biomass gasification system,” *Dissertation*, 2006.
- [23] S. Kern, C. Pfeifer, and H. Hofbauer, “Gasification of wood in a dual fluidized bed gasifier: Influence of fuel feeding on process performance,” *Chemical Engineering Science*, vol. 90, pp. 284–298, 3 2013.
- [24] I. Yasui, M. Ikematsu, S. Hidaka, K. Yumoto, and A. Owatari, “Clean fuel,” *Petrotech*, vol. 23, p. 260, 4 2000.
- [25] K. Zhang, J. Chang, Y. Guan, H. Chen, Y. Yang, and J. Jiang, “Lignocellulosic biomass gasification technology in China,” *Renewable Energy*, vol. 49, pp. 175–184, 1 2013.
- [26] A. M. Mauerhofer, F. Benedikt, J. C. Schmid, J. Fuchs, S. Müller, and H. Hofbauer, “Influence of different bed material mixtures on dual fluidized bed steam gasification,” *Energy*, vol. 157, pp. 957–968, 8 2018.
- [27] M. Kaltschmitt, H. Hartmann, and H. Hofbauer, “Energie aus Biomasse,” pp. 617–619, 2016.
- [28] M. Kolbitsch, “First fuel tests at a novel 100 kWth dual fluidized bed steam gasification pilot plant,” *Dissertation*, pp. 75–78, 6 2016.

- [29] M. Kraussler, M. Binder, and H. Hofbauer, “2250-h long term operation of a water gas shift pilot plant processing tar-rich product gas from an industrial scale dual fluidized bed biomass steam gasification plant,” *International Journal of Hydrogen Energy*, vol. 41, pp. 6247–6258, 4 2016.
- [30] M. Kaltschmitt, H. Hartmann, and H. Hofbauer, “Energie aus Biomasse,” pp. 616–617, 2016.
- [31] D. Porbatzki, M. Stemmler, and M. Müller, “Release of inorganic trace elements during gasification of wood, straw, and miscanthus,” *Biomass and Bioenergy*, vol. 35, pp. S79–S86, 10 2011.
- [32] M. Kolbitsch, “First fuel tests at a novel 100 kWth dual fluidized bed steam gasification pilot plant,” *Dissertation*, pp. 59–63, 2016.
- [33] D. Kadlez, K. Fürsatz, and F. Benedikt, “Validation of first test runs for a 1 MW DFB demonstration plant at Simmeringer Haide,” tech. rep., TU Wien, Vienna, 7 2022.
- [34] J. I. Arranz, M. T. Miranda, I. Montero, F. J. Sepúlveda, and C. V. Rojas, “Characterization and combustion behaviour of commercial and experimental wood pellets in South West Europe,” *Fuel*, vol. 142, pp. 199–207, 2 2015.
- [35] T. Proell and H. Hofbauer, “Development and application of a simulation tool for biomass gasification based processes,” *International Journal of Chemical Reactor Engineering*, vol. 6, pp. 3–5, 2008.
- [36] S. Mueller, J. Fuchs, J. C. Schmid, F. Benedikt, and H. Hofbauer, “Experimental development of sorption enhanced reforming by the use of an advanced gasification test plant,” *International Journal of Hydrogen Energy*, vol. 42, pp. 29694–29707, 12 2017.
- [37] J. C. Schmid, F. Benedikt, J. Fuchs, A. M. Mauerhofer, S. Müller, and H. Hofbauer, “Syngas for biorefineries from thermochemical gasification of lignocellulosic fuels and residues—5 years’ experience with an advanced dual fluidized bed gasifier design,” *Springer*, pp. 2422–2424, 9 2014.
- [38] B. Wojnicka, M. Sciazko, and J. C. Schmid, “Modelling of biomass gasification with steam,” *Biomass Conversion and Biorefinery*, 2019.

- [39] D. Bostroem, N. Skoglund, A. Grimm, C. Boman, M. Oehman, M. Brostroem, and R. Backman, “Ash transformation chemistry during combustion of biomass,” *Energy and Fuels*, vol. 26, pp. 85–93, 1 2012.
- [40] A. Aghaalikhani, J. C. Schmid, D. Borello, J. Fuchs, F. Benedikt, H. Hofbauer, F. Rispoli, U. B. Henriksen, Z. Sárossy, and L. Cedola, “Detailed modelling of biomass steam gasification in a dual fluidized bed gasifier with temperature variation,” *Renewable Energy*, vol. 143, pp. 703–718, 12 2019.
- [41] M. Stidl, “Prozesssimulation von spezifischen Anwendungsfällen der Zweibett-Wirbelschicht-Dampfvergasungs-Technologie für die Papier- und Zellstoffindustrie,” *Ph.D. Thesis*, p. 112, 2012.
- [42] A. Li, H.-L. Liu, H. Wang, H.-B. Xu, L.-F. Jin, J.-L. Liu, and J.-H. Hu, “Effects of Temperature and Heating Rate on the Characteristics of Molded Bio-char,” *BioResources*, vol. 11, no. 2, pp. 3259–3274, 2016.
- [43] C. Guizani, M. Jeguirim, S. Valin, L. Limousy, S. Salvador, and S. S. Biomass, “Biomass Chars: The Effects of Pyrolysis Conditions on Their Morphology, Structure, Chemical Properties and Reactivity,” *Structure, Chemical Properties and Reactivity. Energies, MDPI*, vol. 10, no. 6, 2017.
- [44] M. Kolbitsch, “First fuel tests at a novel 100 kWth dual fluidized bed steam gasification pilot plant,” *Dissertation*, pp. 75–78, 2016.
- [45] V. Wilk and H. Hofbauer, “Conversion of fuel nitrogen in a dual fluidized bed steam gasifier,” *Fuel*, vol. 106, pp. 793–801, 4 2013.
- [46] M. Kaltschmitt, H. Hartmann, and H. Hofbauer, “Energie aus Biomasse,” pp. 1543–1544, 2016.
- [47] M. Kaltschmitt, H. Hartmann, and H. Hofbauer, “Energie aus Biomasse,” pp. 1633–1634, 2016.
- [48] J. Hongrapipat, S. Pang, and W. L. Saw, “Removal of NH<sub>3</sub> and H<sub>2</sub>S from producer gas in a dual fluidised bed steam gasifier by optimisation of operation conditions and application of bed materials,” *Biomass Conversion and Biorefinery*, vol. 6, pp. 105–113, 3 2016.

- [49] I. Gulyurtlu, F. Pinto, H. Lopes, R. N. André, M. Dias, and I. Cabrita, “Prediction of H<sub>2</sub>S and HCl formation during RDF and co-gasification in fluidized bed,” *16th European Biomass Conference & Exhibition*, 2008.
- [50] H. Kuramochi, W. Wu, and K. Kawamoto, “Prediction of the behaviors of H<sub>2</sub>S and HCl during gasification of selected residual biomass fuels by equilibrium calculation,” *Fuel*, vol. 84, pp. 377–387, 3 2005.
- [51] M. Kaltschmitt, H. Hartmann, and H. Hofbauer, “Energie aus Biomasse,” pp. 1683–1686, 2016.
- [52] S. I. Ngo, T. D. Nguyen, Y. I. Lim, B. H. Song, U. D. Lee, Y. T. Choi, and J. H. Song, “Performance evaluation for dual circulating fluidized-bed steam gasifier of biomass using quasi-equilibrium three-stage gasification model,” *Applied Energy*, vol. 88, no. 12, pp. 5208–5220, 2011.
- [53] M. Binder, “Long term performance of an Fe/Cr based water gas shift catalyst processing tar-rich wood gas,” *Diplomarbeit*, pp. 48–55, 2015.
- [54] M. Kaltschmitt, H. Hartmann, and H. Hofbauer, “Energie aus Biomasse,” pp. 669–674, 2016.
- [55] X. Wang and M. Economides, “Gas-To-Liquids (GTL),” *Advanced Natural Gas Engineering*, pp. 243–287, 2009.
- [56] X. Yan, Y. Liu, B. Zhao, Z. Wang, Y. Wang, and C. J. Liu, “Methanation over Ni/SiO<sub>2</sub>: Effect of the catalyst preparation methodologies,” *International Journal of Hydrogen Energy*, vol. 38, pp. 2283–2291, 2 2013.